Nanoscale

FEATURE ARTICLE

Cite this: *Nanoscale*, 2016, **8**, 9890

Recent developments in the layer-by-layer assembly of polyaniline and carbon nanomaterials for energy storage and sensing applications. From synthetic aspects to structural and functional characterization

Waldemar A. Marmisollé*[a,b] and Omar Azzaroni*[a,b]

The construction of hybrid polymer–inorganic nanoarchitectures for electrochemical purposes based on the layer-by-layer assembly of conducting polymers and carbon nanomaterials has become increasingly popular over the last decade. This explosion of interest is primarily related to the increasing mastery in the design of supramolecular constructs using simple wet chemical approaches. Concomitantly, this continuous research activity paved the way to the rapid development of nanocomposites or "nanoblends" readily integrable into energy storage and sensing devices. In this sense, the layer-by-layer (LbL) assembly technique has allowed us to access three-dimensional (3D) multicomponent carbon-based network nanoarchitectures displaying addressable electrical, electrochemical and transport properties in which conducting polymers, such as polyaniline, and carbon nanomaterials, such as carbon nanotubes or nanographene, play unique roles without disrupting their inherent functions – complementary entities coexisting in harmony. Over the last few years the level of functional sophistication reached by LbL-assembled carbon-based 3D network nanoarchitectures, and the level of knowledge related to how to design, fabricate and optimize the properties of these 3D nanoconstructs have advanced enormously. This feature article presents and discusses not only the recent advances but also the emerging challenges in complex hybrid nanoarchitectures that result from the layer-by-layer assembly of polyaniline, a quintessential conducting polymer, and diverse carbon nanomaterials. This is a rapidly developing research area, and this work attempts to provide an overview of the diverse 3D network nanoarchitectures prepared up to now. The importance of materials processing and LbL integration is explored within each section and while the overall emphasis is on energy storage and sensing applications, the most widely-used synthetic strategies and characterization methods for "nanoblend" formation and performance evaluation are also presented.

Received 24th November 2015,
Accepted 7th January 2016

DOI: 10.1039/c5nr08326e

www.rsc.org/nanoscale

1. Introduction

The integration of hybrid polymer–inorganic nanoarchitectures in electrochemical interfaces has attracted considerable attention and consequently significant progress in a number of key areas has been achieved over the past few years. Part of the appeal of designing electrochemical devices with nanoscale organized materials is that they offer the possibility of manipulating functional building blocks at the molecular level, this being a target in many applications where high performance is needed. Research efforts on this matter are often referred to as "*nanoarchitectonics*", a term popularized by Ariga and his co-workers.[1–7] In the case of electrochemical devices, for example, the interest in such manipulation is related to the enhancement of the energy storage characteristics of batteries or the improvement of the electronic readout signal of biosensors.

Among a wide variety of versatile materials used for electrochemical devices, carbon-based materials, predominantly represented by carbon nanotubes and nanographene, have been used as the building blocks of different electrochemical interfaces due to their unique electrical, mechanical, and chemical properties.[8–10] However, in spite of these promising prospects there remains a critical need to integrate additional building blocks into carbon-based electrochemical devices in order to develop their full potential.[9] For example, the application of nanographene in supercapacitors is somewhat limited due to their low capacitance. In order to overcome this limitation, materials scientists have combined nanographene

[a]*Instituto de Investigaciones Fisicoquímica Teóricas y Aplicadas (INIFTA), Departamento de Química, Facultad de Ciencias Exactas, Universidad Nacional de La Plata, CONICET, C.C. 16 Suc. (1900) La Plata, Argentina*
[b]*Consejo Nacional de Investigaciones Científicas y Técnicas (CONICET), Argentina. E-mail: azzaroni@inifta.unlp.edu.ar, wmarmi@inifta.unlp.edu.ar; http://softmatter.quimica.unlp.edu.ar*

with conducting polymers with the aim of taking advantage of each component and improving the performance of the electrochemical device.

Bringing conducting polymers into the game opened up a new horizon: the possibility to create three-dimensional (3D) multicomponent carbon-based network architectures displaying tailored electrical, electrochemical and transport properties.[11] Such 3D nanoarchitectures involve the phase-separated coexistence of conducting polymer domains and carbon nanomaterials operating as nanoelectrodes. This ultimately leads to the construction of advanced interconnecting conductive networks displaying built-in electrochemical functions.[12,13] In this context, it is evident that new properties are bound to arise not only from the synergy of both kinds of components, but also from their spatial configuration – a feature very suitable for flexible integrated devices.

Depending on the purpose of these hybrid network architectures hosted on electrode supports, conducting polymers can facilitate better capacitance values by exploiting their faradaic reactions or improve the electronic communication between transduction elements and the electrode surface due to their reversible redox activity. Within this framework, polyaniline (Pani) has long been considered the quintessential conducting polymer for energy storage and conversion purposes due to their high conductivity values, remarkable pseudocapacitive properties, reversible faradic reactions and ease of synthesis. One of the distinctive features of Pani is its electronic conductivity and the possibility of controlling its conducting states by manipulating the protonation and the oxidation state of the polymer chains. With these potential advantages and the promise of numerous tangible benefits, the formation of hybrid networks constituted of carbon nanotubes and/or nanographene and electrochemically active Pani has found incredible resonance within the nanoscience and materials science communities.

Clearly, the control of composition, morphology and architecture of the hybrid Pani/carbon nanomaterial networks is an essential cornerstone for transforming the polymer-inorganic nanocomposite into nanoarchitectured electrochemical interfaces, this being one of the biggest challenges associated with the design of electrochemical devices for energy storage and sensing applications.[13,14] For instance, even though considerable progress has been observed in this direction, many of the reported hybrid films lack adequate and precise control over the film architecture. This fact concomitantly leads to a loss of the active surface and intimate contact between polymeric and inorganic counterparts. The realization of hybrid interconnected conducting networks through the formation of nanoscale uniform blends of nanographene or carbon nanotubes and Pani is not trivial and proves to be quite challenging. As a strategy for advancing in the controllable preparation of such hybrid interfaces several research groups started to explore the possibility of using layer-by-layer (LbL) assembly to integrate the complex functions of both nanomaterials with nanometer-scale control over the film composition and structure.[9] This technique was first proposed by Iler in 1966, and then rediscovered by Decher and Hong in 1991,[15–18] and is based on the alternate deposition of polyanions and polycations on a charged surface in order to form polyelectrolyte multilayers in a controlled manner.

Today this technique has taken on a new dimension and allows the incorporation of diverse nanostructures, including

Waldemar A. Marmisollé

Waldemar A. Marmisollé was born in Junín (Buenos Aires, Argentina) in 1984. He studied chemistry at the Universidad Nacional de La Plata (UNLP) receiving his degree in 2007 and his PhD in chemistry in 2011. He performed post-doctoral work at the Universidad de Buenos Aires (UBA) and he is now a fellow member of CONICET working at the Soft Matter Laboratory of the Instituto de Investigaciones Fisicoquímicas Teóricas y Aplicadas (INIFTA) (UNLP-CONICET). His research interests include conducting polymers and soft matter electrochemistry.

Omar Azzaroni

Omar Azzaroni studied chemistry at the Universidad Nacional de La Plata (UNLP) (Argentina), receiving his Ph.D. in 2004. His postdoctoral studies were carried out at the University of Cambridge (UK) (2004–2006, Marie Curie Research Fellow) and the Max Planck Institute for Polymer Research (Germany) (2007, Alexander von Humboldt Research Fellow). He was then appointed as Max Planck Partner Group leader from 2009 until 2013. He has served as Vice-Director of the Instituto de Investigaciones Fisicoquímicas Teóricas y Aplicadas (INIFTA) (2012–2015). He is currently a fellow member of CONICET and head of the Soft Matter Laboratory of INIFTA. Since 2009, he is also Adjunct Professor of Physical Chemistry at UNLP. His research interests include nanostructured hybrid interfaces, supra- and macromolecular materials science and soft nanotechnology. More information can be found at: http://softmatter.quimica.unlp.edu.ar

carbon nanotubes, nanoparticles, and diverse polymers on virtually any surface.[19–21] One of the most attractive features of the LbL technique is its capability to manipulate the structure and composition of the generated nanoarchitectures by controlling the layering sequence of the chosen materials.[22,23] Indeed, it is now clear that the successful marriage of carbon nanomaterials and Pani, not to mention the transformation of such hybrid assemblies into nano-organized and compartmentalized devices, can be largely attributed to the timely implementation of the LbL technique as a key enabling technology.

Our aim with this work is to provide the reader with an overview of current research efforts devoted to the construction of multilayered hybrid assemblies constituted of polyaniline and diverse carbon nanomaterials, with particular attention to properties and functions, and to strengthen the contacts between the electrochemical and nanoscience communities sharing an interest in energy storage and sensing applications. Although the text covers a wide range of experimental systems recently reported in the literature, it does not even attempt to be a comprehensive review on the subject. Instead, we intended to give the reader a notion of the level of ingenuity reached by colleagues working in this area as well as highlight critical aspects related to structural and functional characterization of the hybrid multilayered structures.

We hope that the review will be useful as a reference not only for new and experienced researchers in the field, but also for graduate students and postdoctoral fellows who are interested in exploring the convergence of electrochemistry and nanoscience into a new frontier of materials science. In the most optimistic sense, the experimental systems described herein not only in themselves provide novel approaches to sensing platforms and energy storage devices, but also may lead to new ideas, concepts and notions in supramolecular materials science.

1.1. Polyaniline

Conducting polymers (CPs) have received great attention in the last few decades owing to their excellent electronic and electrochemical properties.[24–26] Among CPs, polyaniline (Pani) has been one of the most studied cases owing to its superior electronic conductivity, inexpensive simple synthesis and high stability under ambient conditions.[27–29] Pani also presents other advantages such as tunable properties[30,31] and the possibility of further chemical modifications,[32] which have propelled its application in different areas.

Pani has become a promising material in energy storage applications as it has one of the highest theoretical specific pseudocapacitances (2000 F g^{-1}) caused by its fast and reversible redox transformations and high surface area.[33]

Pani has also been extensively employed for biosensors[31] and other biodevices[34] as it can provide an adequate non-denaturing environment for the immobilization of enzymes and proteins and simultaneously it can act as a physicochemical transducer of the chemical signals into a measurable electrical response, or simply mediate the electron transport to the electrode.[31,35,36]

1.1.1. Redox states of Pani. The tetramer of Pani is considered to be the redox unit.[37,38] This unit can be found in several oxidation states. The totally reduced state consists of just benzenic units and it is called leucoemeraldine (L). It is usually in its basic form (LB), but in highly acidic solutions it becomes protonated (pK_a about 1)[39] and it is then referred to as leucoemeraldine salt (LS). The oxidation of leucoemeraldine leads to the emeraldine form (E), where a quinone-imine structure is obtained by removing two electrons from the benzenic moiety. Emeraldine can exist in its base form (EB) or be protonated to the emeraldine salt (ES). Further oxidation yields the pernigraniline form (P) in which the other benzenic unit is converted into quinone-imine. Again, it can be in its base (PB) or salt form (PS). The chemical structure of the Pani redox forms is depicted in Scheme 1. These three states are widely recognized,[37,38,40,41] but sometimes other intermediate redox states are defined, such as protoemeraldine[42,43] and nigraniline.[37]

The PS form is not stable in acidic media and further oxidation of E generally leads to a degradation of the polymer. On the contrary, the interconversion between the L and E forms is highly reversible in acidic media. The protonation (sometimes referred as p-doping) of the EB form leads to a dicationic structure that is the chemical equivalent to the bipolaron used in the physical description. This structure can be internally transformed into a species with radical cations (the chemical equivalent of polarons), whose electrons are delocalized along the polymer chain. In doped Pani, polarons are more stable than bipolarons and they are responsible for the high electronic

Scheme 1 Chemical structures of redox forms of Pani.

conductivity.[27,31,44] The radical cation acts as a hole in the charge transport mechanism. This electronic scheme was proposed by MacDiarmid and co-workers in the 80s.[44]

1.2. Carbon nanomaterials: nanotubes and graphene

Carbon nanomaterials refer to the nanostructures made by sp^2 graphitic carbon atoms and include fullerenes, carbon nanotubes and graphene-like materials.[45,46] Their particular electronic structure made them interesting materials in many application fields such as energy storage,[47–50] sensors[51] and optoelectronic devices.[46]

1.2.1. Carbon nanotubes. Carbon nanotubes (CNTs) are hollow cylindrical tubes made of one (called single-walled nanotubes, SWNTs) or more layers of graphitic carbon atoms (called multi-walled nanotubes, MWNTs). Due to their particular chemical structure, they present exceptional mechanical and electrical properties[52] that have propelled their application in several technological fields.[53]

1.2.2. Graphene (Gr), graphene oxide (GO) and reduced graphene oxide (rGO). The IUPAC defines a graphene (Gr) layer as "a single carbon layer of the graphite structure, describing its nature by analogy to a polycyclic aromatic hydrocarbon of quasi infinite size".[54] However, the term is widely employed in the literature to refer to a variety of graphite-like materials.[55] Several top-down and bottom-up methods of preparation of these materials have been described.[56,57] One of the most employed top-down methods consists of the oxidative exfoliation of graphite. In this procedure, oxygen groups are intercalated within the graphite layers by treatments with oxidizing agents in concentrated nitric and sulfuric acids. The intercalation causes an increase of the interlayer distance and a decrease of the staking interaction that allows the exfoliation by ultrasonication to produce sheets of graphene with a high proportion of oxygen functionalities which is generally called graphene oxide (GO). As GO is obtained in a liquid dispersion, the results of this method are interesting for the large-scale production of graphene materials with good processability. The proportion and nature of these oxygen-containing groups depends on the preparation method, but typically the C/O ratio is about 2.[55] Most studies on the LbL assembly of Pani and graphene-like materials actually involve the usage of GO as the starting material, so we will focus on this material. Particularly, most of the studies in this review employ GO obtained by the method introduced by Hummers in 1958 and recently improved by Tour,[58] which requires potassium permanganate as the oxidizing agent.[59]

Materials more similar to the canonical graphene can then be obtained by reduction of GO, although it is not possible to achieve a complete reduction.[55] The proportion of oxygen in the reduced GO (rGO) depends on the reduction method, which basically can be thermal (annealing at high temperature), chemical or electrochemical.[55]

The use of graphene-like materials in electrochemistry is vast as has been recently reviewed by Pumera.[55] Additionally, GO presents an inherent electrochemical response owing to the presence of electroactive oxygen functionalities.[55]

2. LbL assemblies for energy and sensing

2.1. Pani in LbL assemblies

The first studies on the use of Pani and related conducting polymers in LbL assemblies were published by Rubner's group in the middle 90s.[60–62] They introduced a method to produce dispersions of Pani that are stable for more than one day,[61] which would be used in many of the later studies on LbL of Pani with little modification. Briefly, the chemical synthesis of Pani is performed by oxidation with ammonium persulfate (APS) in acidic solution. The resulting emeraldine salt (ES) is converted into the emeraldine base (EB) by treatment with NH_4OH, and dried in a vacuum. The EB powder is dissolved in dimethylacetamide (DMAc) by stirring and sonication and the remaining particulates are filtered. Although *N*-methylpyrrolidone (NMP) has also been used to dissolve EB,[63] it was reported to be more tightly bound to Pani and hence it results in being difficult to eliminate from the assemblies, yielding less conductive layers.[62] This DMAc organic solution is diluted with acidic water to form an aqueous solution of pH about 2.5. This solution is said to be stable between pH 2.5 and 4 and some authors have even recommended 2.8 as the optimal pH.[64] Rubner and coworkers studied the dip-coating assembly of Pani with polystyrene sulfonate (PSS) by UV-visible absorption and the effect of Pani concentration. They found that, although the thickness and absorbance linearly depend on the dipping cycles, the in-plane conductivity (4-probes method) increases with the number of bilayers until about 6 bilayers and then it remains in its bulk value. This suggests that the deposition of Pani is not in complete layers and a percolation of the successive added polymer occurs. A granular structure was also observed in further studies on Pani/PSS assemblies.[64] They have also shown that Pani can be deposited in LbL films using non-ionic polymers by hydrogen-bonding interactions of dedoped Pani.[62]

The assembly of Pani and PSS was further studied by different groups, focusing on the morphology and conductivity dependence on preparation conditions,[65] and its electrochemical degradation monitored by electrochemical impedance spectroscopy (EIS).[66] Moreover, the assembly of Pani/PSS has also been grown on polystyrene spheres to yield LbL hollow spheres after PS dissolution.[67] It has also been assembled on nylon films.[68] The assembly and electrochromic evaluation of Pani/PSS LbL films has even been proposed as pre-degree laboratory experience.[69]

Several other polyanions have been employed as counterparts in different LbL assemblies with Pani. Pani (from NMP dispersions) and poly(acrylic acid) (PAA) LbL films have been showed to be both electroactive[70] and electrochromic[71] in neutral media and have been employed for potentiometric pH sensing[72] and amperometric sensing of H_2O_2.[73] Enzymatically synthesized Pani and poly(glutamic acid) LbL films were tested for capacitive applications.[74] Pani and anionic azopolyelectrolytes were also assembled into electroactive and electrochromic

films.[75] The electrical properties of poly(vinylsulfonic acid) and Pani LbL assemblies have also been studied.[76] The LbL assembly of Pani and oligonucleotides has produced electroactive films in neutral media, although less electroactive than Pani/PSS films.[77] Even complexes of Pani and gum Arabic assembled LbL with PSS have shown good electroactivity and stability.[78]

Furthermore, the assembly of substituted polyanilines has been reported. Particularly investigated has been the case of sulfonated Pani which bears a negative net charge and hence can be assembled with its cationic counterparts. The presence of anionic groups also improves the solubility and processability and they also extend the electroactive pH range as they act as dopants (self-doping).

Poly(anilinesulfonic acid) (PASA) has been assembled with a poly(amidoamine) dendrimer (PAMAM) from aqueous solution yielding electroactive films.[79] The changes in the resistance of LbL films of PASA and polyallylamine (PAH) have been employed for humidity sensors.[80] Owing to its electroactivity in neutral solutions, PASA has been extensively employed for the electrochemical LbL assembly of proteins, such as cytochrome,[81,82] sulfite oxidase,[83] xantine oxidase,[84] and bilirubin oxidase.[85,86] On the other hand, poly(aniline-*N*-butylsulfonate) (PANBS) has been assembled with Pani and other cationic polyelectrolytes as electrochromic films in organic electrolytes.[87]

2.1.1. Pani with other conducting polymers. The first electrochromic device based on the LbL assembly of Pani and poly(3,4-ethylenedioxythiophene (PEDOT) was reported by Hammond.[88] There, Pani was assembled by using poly(2-acrylamido-3-methyl-1-propanesulfonic acid) (PAMPS) as the counterpart. The LbL films of Pani and polyanions were loaded with Pt to yield composites with good electronic and ionic conductivities.[89] The response of the modified electrodes was comparable to that of bulk Pt.

Pani (Rubner's method) and post-polymerization-sulfonated Pani (sPani) were assembled LbL from aqueous dispersions yielding electroactive films that were studied by electrochemically-coupled surface plasmon resonance (SPR)[90] and tested as electroactive films for electrochromic devices.[91] Even, the effect of high applied pressures on this LbL has been studied by SPR.[92] The assemblies of Pani and sPani also showed good electroactivity in neutral solution and catalyzed the electro-oxidation of NADH.[93]

More recently, the negative complex of Pani synthesized by template polymerization with poly(2-acrylamido-2-methyl-1-propanesulfonic acid) has been assembled with Pani (Rubner's method) to yield electroactive films that were tested in Li cells.[94] They presented better charge capacity and cycle life than LbL without all electroactive layers.

2.1.2. Other assemblies LbL with Pani and different materials. Owing to its interesting electronic and electrochemical properties, Pani has been extensively employed in the construction of LbL assemblies with other inorganic nanomaterials as counterparts for different applications.

Pani has been assembled with citrate capped-Au NPs to yield conductive and electroactive films,[95] which have also been employed for electrochemical sensing of dopamine and uric acid in neutral solution.[96] The assemblies with mercaptosuccinic acid capped-Au NPs were employed for NADH electrooxidation and detection of DNA hybridization.[97] The assemblies of Pani with Pd NPs, by LbL and reduction of Pani and $PdCl_6^{2-}$,[98] as well as PdO NPs[99] have been employed for hydrazine oxidation electrocatalysis.

A wide range of inorganic materials has been also employed in LbL films with Pani: V_2O_5 xerogels for electrochromic[100,101] and Li intercalation devices and energy storage;[102–105] Prussian Blue nanocrystals for electrochromic devices;[106] isopolymolybdic acid in films sensitive to humidity and different gases;[107] Keggin-type polyoxometalates have also yielded conductive films by LbL deposition;[108] and the LbL assemblies with phosphotungstic acid have been tested as proton-conducting membranes to be applied in polymer electrolyte membranes (PEMs);[109] NbO_6 nanoscrolls have also been assembled LbL to produce electrochromic films;[110] films with MnO_2 resulted in photoactivity and were employed for the photocatalytic degradation of a dye;[111] montmorillonite clay nanosheets were assembled LbL to modify electrodes that were then employed for heavy metal ion sensing by square-wave voltammetry.[112]

2.2. LbL of Pani and CNTs

Scheme 2 summarizes the construction and applications of LbL assemblies of Pani and carbon nanotubes reported in this article.

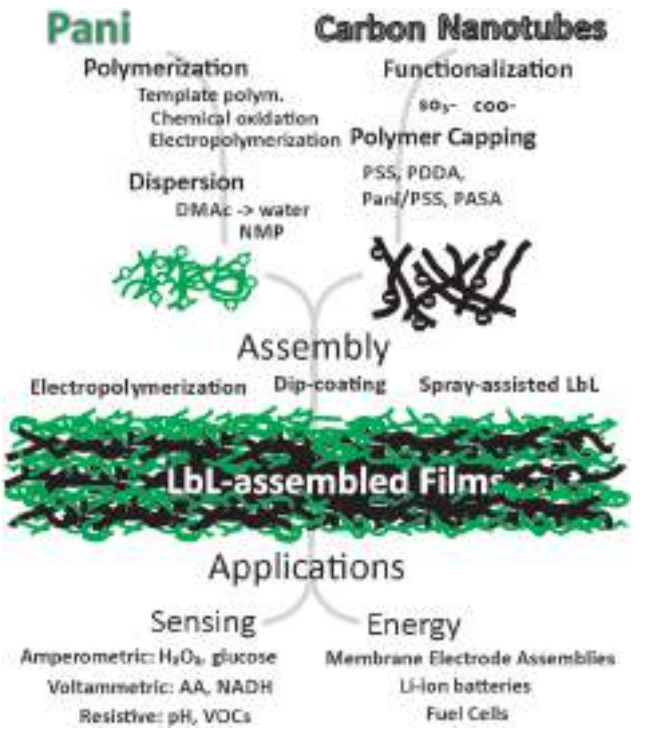

Scheme 2 Construction and applications of the LbL films of Pani and CNTs.

2.2.1. Conductive film-resistance as a responsive property. Feng *et al.* showed that MWNTs modified with carboxylic and sulfonic groups (s-MWNTs) dispersed in water can be assembled with Pani from a NMP dispersion by dip-coating on amino-functionalized non-conducting substrates.[113] The interaction of Pani with the anionic groups of the s-MWNTs was proved by UV-vis spectral changes. The results suggest that the s-MWNTs effectively act as the dopant of the conducting form of Pani, yielding an increased electrical conductivity at room temperature.

The electronic conductivity in the LbL arrays was further studied by Kovtyukhova *et al.*[114] In this work, Pani from a DMF solution was deposited by dip-coating in a LbL film with oxidized SWNTs (bearing-COOH groups) on Au substrates.[114] The electrostatic interaction between amine/imine groups in Pani and COO^- in the SWNTs was confirmed by FTIR and XPS, although they also suggest the formation of charge transfer complexes between the π-systems of both components. They found that the conductivity was highly anisotropic; the lateral (in the horizontal plane) dominated by the CNTs and the transversal (in the vertical plane) limited by the polymer (Fig. 1). The small size and strong adhesion between the oxidized SWNTs within a layer would be responsible for the excellent lateral electronic conductivity.

The electrostatic interactions between Pani and oxidized MWNTs were also employed to synthesize composites from dispersions of both components.[115] The composites showed an intimate connection between Pani and the MWNTs as confirmed by Raman and FTIR. Just a low proportion of MWNTs is necessary to effectively connect the Pani fibers producing a material with enhanced electronic properties. In a different approach the LbL method was employed to decorate MWNTs with a combination of poly(aniline-*co*-anisidine) and PSS as a way to produce conductive and dispersible composites (Fig. 2).[116] More recently, the electrical properties of other LbL assemblies have been reported. MWNTs were modified by adsorption of poly(diallyldimethylammonium chloride) (PDDA) and assembled with Pani/PSS complexes,[117] although better conductivities were achieved by assembling PDDA-coated MWNTs and Pani/PSS-coated MWNTs.

Based on the pH response of a Pani film electrosynthesized on a polyethylene terephthalate (PET) plate coated with SWNTs,[118] Loh *et al.* prepared an LbL assembly employing Pani and purified SWNTs coated with PSS on a glass plate.[119] The change of a 100 bilayer film resistance with pH was linear in the acidic range but non-linear in the basic range. However, the time response was lower than that found in previous studies.

The same LbL assembly has been employed as a pH sensor by electrical impedance tomography.[120] The 2D spatial distribution of conductivity of the LbL film (sensing skin) was measured when exposed to different pH solutions. The conductivity changes were almost linear in the whole pH range (1–13) with similar sensitivities. In another work, the LbL film of Pani and PSS-SWNTs was employed as a layer with resistance sensitivity to pH with a near linear response to be

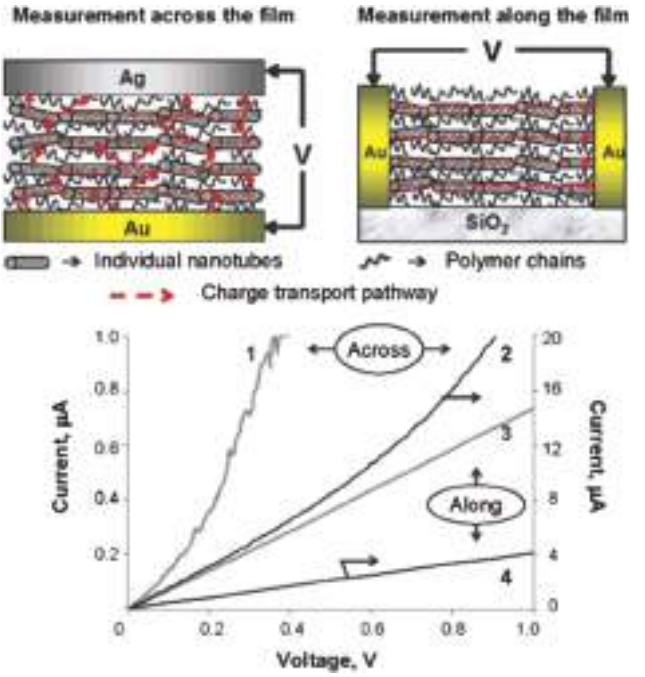

Fig. 1 Schematic representation and experimental determination of the anisotropic conductivity in Pani/SWNT LbL assembled films. Reprinted with permission from ref. 114. Copyright (2005) American Chemical Society.

implemented in a wireless pH sensor.[121] More recently, the effect of pH on DC resistance and EIS response of similarly constructed LbL assemblies of Pani and PSS modified SWNTs on glass has been studied.[122] Both the DC resistances and the resistors of the fitted equivalent circuit linearly depend on pH but also two pH ranges are observed, being more sensitive in the basic range.

In a different approach, PSS-doped Pani NPs were assembled with MWNTs by a spray-assisted LbL process.[123] The films were tested as chemo-resistive sensors for volatile organic compounds. The composite films of Pani and MWNTs present both higher sensitivity and selectivity than those formed by just Pani, demonstrating a positive synergy.

2.2.2. Electroactive films for sensing. The first electrochemically active LbL assembly of Pani and CNTs was reported by Knoll's group in 2005.[124] They assembled Pani from an aqueous dispersion of the commercial Pani and SWNTs capped with poly(aminobenzenesulfonic acid) by dip-coating on MPS-modified Au electrodes. The growth of the assembly was monitored by SPR and electrochemistry. The resulting films were electroactive in neutral solution and the voltammetric charge increased with the number of bilayers, which indicates a good electronic connection between the successive layers. Just one pair of voltammetric peaks was observed due to the overlap of both redox couples of Pani at this pH, as has been observed for LbL of Pani and Au NPs.[97] These films also showed electrocatalysis of NADH oxidation at neutral pH, with a linear increase of the voltammetric peak current on NADH concentration.

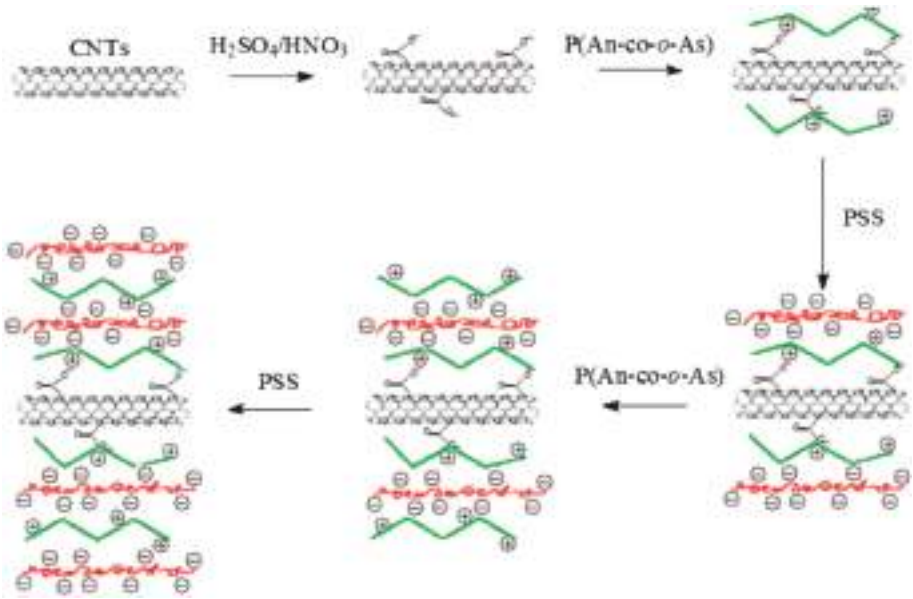

Fig. 2 Schematic representation of the LbL capping of CNTs. Reprinted with permission from ref. 116. Copyright (2008) American Chemical Society.

Another strategy was presented in the same year by Qu *et al.*[125] They cast an ethanolic dispersion of oxidized MWNTs (COOH-bearing) on a glassy carbon electrode and then electropolymerized Pani on it by several voltammetric cycles in aniline acidic solution. The successive bilayers were formed by successive depositions of CNTs and electropolymerizations of aniline. This assembly was tested for the amperometric electrooxidation of H_2O_2 in PBS buffer at 0.4 V *vs.* SCE. They also deposited Choline Oxidase (CHOD) on these films by casting a dispersion of CHOD cross-linked to BSA by glutaraldehyde. The resulting modified electrode showed a linear amperometric response to the increasing concentration of choline at 0.4 V in neutral solutions.

In another case, LbL films of Pani and PSS-capped MWNTs were formed on a glassy carbon electrode by dip-coating from aqueous dispersions.[126] The film was electroactive in neutral PBS solution with a quasi-reversible unique couple at about 0 V *vs.* SCE and was shown to amperometrically sense H_2O_2 at −0.1 V. The electrochemically active material increased with the number of bilayers until 7 bilayers, but a limiting amount was obtained for further deposition cycles.

More recently, negatively charged (COO^- bearing) MWNTs have been assembled with Pani upon ITO to yield electroactive films.[127] Raman and SEM studies indicated a homogeneous assembly. The modified electrodes were evaluated for the electrooxidation of 2-chlorophenol, showing a synergistic effect of Pani and CNTs. The application of square wave voltammetry allowed the determination of 2-chlorophenol up to the ppm level.

In another work, the LbL assembly of Pani-capped MWNTs and PSS resulted in electroactive films with better performance than Pani/PSS films, without a significant modification of the film morphology.[128] The UV-visible measurements indicate a linear increase of the deposited material with the number of bilayers, whereas the voltammetric response shows a good electrochemical connection. The presence of the MWNTs promotes higher charge transfer efficiencies.

Even more complex architectures were assembled. NH_2-functionalized MWNTs were mixed with aniline and aminothiophenol and deposited on an ITO electrode.[129] Then an electropolymerization of the deposited arylamines was performed. Au NPs and then GOx were fixed on this layer. The same procedure was repeated several times for the successive bilayers. They found a synergistic contribution of all components to obtain high electron transfer rate constants. These assemblies responded rapidly to glucose in solution and an amperometric linear correlation with glucose concentration was obtained at 0.4 V (*vs.* Ag/AgCl). The presence of CPs and CNTs would allow an efficient electric connection between the prosthetic groups in GOx and the electrode and would promote rapid electron transfer. The presence of the conducting polymer was shown to reduce the detection limit and enhance sensitivity compared to similar LbL arrays without Pani.

2.2.3. LbL in energy devices. The LbL assemblies of Pani and CNTs were also evaluated as membrane electrode assemblies (MEAs) in fuel cells.[130] SWNTs decorated with Pt NPs by a supercritical fluid method were capped with Nafion to obtain stable dispersions in water/ethanol mixtures. These dispersions were employed to grow LbL assemblies in a dip-coating method by employing acidic aqueous dispersions of Pani as the positive counterpart. The LbL prepared as free self-standing films were constructed into membrane electrode assemblies and tested in a fuel cell station. By using a conduct-

ing polymer it was not necessary to add carbon nanomaterials to the positive layer to obtain adequate electrical connectivity. Moreover, owing to the homogeneity achieved by the LbL method, excellent values of Pt utilization (power relative to Pt mass) could be achieved.

In another work, Pani fibers were modified by Pt NP deposition, then they were assembled with Pt NP-modified MWNTs in LbL arrays by spraying from ethanolic solutions on a Nafion membrane.[131] This membrane was tested as MEA in a H_2/air fuel cell yielding high values of Pt utilization. As suggested by previous studies,[132,133] the electronic conductivity would be exclusively due to the presence of CNTs when the percolation limit is exceeded (30% mass) and the CPs would only contribute to the proton conductance in these membranes.

Pt-decorated Nafion-capped MWNTs were also assembled on carbon paper employing Pani as the positive counterpart for being used as catalyzers in biohydrogen fuel cells.[134] The layer of Pani was grown by both chemical and electrochemical polymerizations on top of the MWNT layer. This multilayer assembly showed better catalytic activity for H_2 oxidation than the core–shell assembly of Pani and CNTs, which was attributed to a better contact between the Pani fibers and the Pt-MWNT layer.

The assemblies with CNTs were also employed in Li-ion cells. Chemically synthesized Pani and oxidized MWNTs were assembled by dip-coating on ITO from water dispersions.[135] The films annealed at 180 °C showed better mechanical stability and conductivity. The annealed films also showed a linear increase of thickness on deposition cycles. They presented a cross-linked reticulated structure with nanoporosity and interconnectivity, which enhanced the electron and ionic transport. When tested in a Li-cell, they presented high power density due to the pseudocapacitive reaction of Li cations with anionic groups of the oxidized CNTs and anions with positive charges in Pani fibers.

2.3. GO and rGO in LbL assemblies

As far as we are concerned, the first reports on GO assembled on LbL structures were published by Fendler's group in the middle 90s. They assembled exfoliated GO (2–3 sheets of GO) and PDDA from aqueous solutions. The assembled materials were confirmed by SPR and UV-visible spectroscopy and the LbL structure was studied by X-ray diffraction (XRD). They also reported both chemical and electrochemical reduction of the GO to yield a material with enhanced electronic conductivity.[136] They further prepared similar LbL assemblies with poly(ethylene oxide) (PEO) and PDDA[137] and tested them as electrode materials for Li-ion batteries[138] and even prepared more complex films by assembling Ag NPs capped with GO pellets in an LbL procedure with PDDA.[139]

GO was also shown to form LbL assemblies with PAH on a variety of substrates.[140] The structure of the assemblies depends on the GO dispersion characteristics and they present a diode-like behavior. In another work, the assembly of GO and PDDA was further studied by UV-visible spectroscopy and XRD and then the GO was partially reduced with hydrazine.[141] The LbL assembly of GO and PDDA has also been tested as a humidity responsive film in a quartz crystal microbalance (QCM) sensor[142] and also as an electrochemical supercapacitive film after reduction of the assembled GO.[143] Negative GO has also been assembled with polyethylenimine (PEI)[144] and PAH[145] for different applications.

GO has also been incorporated in the positive layer of the assemblies by a variety of strategies. GO was turned positive by adding a non-covalent CTAB capping. This complex was then assembled LbL with PAA[146] as well as PSS[147] as the negative counterpart by dip-coating from aqueous solutions. Also rGO nano-platelets were grafted by polymerization of PAA or polyacrylamide and then assembled in LbL arrays.[148] The assembly of PAH-rGO and PSS-rGO also yielded conductive films.[149] The assembly of PDDA-rGO and negatively charged rGO on PET substrates produced flexible and transparent conductive plates.[150] Even rGO were deposited by vacuum filtration and then decorated with Au NPs by *in situ* reduction of Au^{3+}, producing a LbL assembly by repetition of these steps.[151]

Since the Nobel Prize in 2010 to Andre Geim and Konstantin Novoselov for their studies on graphene, the presence of graphitic materials in literature has drastically increased, including the works on LbL assemblies containing GO/rGO. In addition, both GO and rGO have been assembled in LbL arrays with a variety of complex organic and inorganic materials. The following are just examples of this wide range of materials and applications.

Single layers of a layered double-hydroxide of Co and Al were assembled with GO employing polyvinyl alcohol (PVA) to stabilize the film, which becomes conductive after chemical reduction of GO.[152] After photocatalytic reduction of the GO, a LbL film of GO and TiO nanosheets with PDDA becomes photoconductive.[153] GO reduced in the presence of positive ionic liquids yielded composites that were assembled LbL with PSS by dip-coating and the films were tested for QCM gas sensing.[154] Gr nanosheets capped by an ionic liquid were assembled with citrate-capped Pt NPs by dip-coating on ITO and the modified electrode was employed for O_2 reduction electrocatalysis in acidic media.[155]

COO^--bearing rGO sheets were assembled with amine-modified rGO by drop-casting in a spin-coater and the resulting conductive film was employed as a transparent electrode in an OLED device.[156] Also COO^--rGO and amine-modified rGO were assembled by dip-coating from water dispersions giving conductive films of controllable thickness.[157] Moreover, COO^--GO and amine-modified GO assemblies were reported to yield transistors with tunable charge transport after thermal reduction.[158]

rGO assembled with an azo-containing cationic copolymer was employed as the electroactive material in an electrochemical double-layer capacitor.[159] Alternating layers of GO and a polyoxometalate cluster assembled with PAH were employed in a thin layer field effect transistor (FET) device after photoreduction of the GO.[160] Free-standing membranes were prepared by LbL deposition of Gr and MnO_2 nanotubes employing an ultrafiltration method and tested as anodes in Li-ion

batteries.[161] Films of PDDA-rGO and negative Fe_3O_4 NPs (1 M NH_4OH) were employed for an amperometric H_2O_2 sensor.[162] On the other hand, rGO was assembled with positive Fe_3O_4 NPs (pH 4 solution) to form films with an enhanced capacitive response in neutral NaCl solutions.[163] Cationic polyelectrolyte-functionalized ionic liquid decorated graphene sheets (PFIL-GS) were assembled with Prussian Blue NPs for the development of an electrochemically-coupled-SPR sensor of H_2O_2. The LbL assembly of GO and Ag^+ cations was reported to yield transparent and electrically conductive films of rGO-Ag NPs after thermal annealing.[164] A uniform film of N and B-codoped-Gr obtained by thermal treatment of a GO/poly (lysine) LbL assembly intercalated by boric acid showed an improved capacitive performance as an active material in a planar microsupercapacitor.[165] GO and cationic terpyridyl-Ru complexes have been shown to be electrochemically active in organic electrolytes and also photoactive, with a synergistic effect between both components.[166]

2.4. LbL of Pani with GO/Gr

The first work on LbL assembly of Pani and GO/Gr was published in 2011.[167] Pani and GO (Hummers' method) were assembled LbL by dip-coating on APTES-modified substrates (Fig. 3). The assemblies were monitored by UV-visible spectroscopy and characterized by AFM. After reduction with HI, the Gr/Pani films presented good electronic conductivities, indicating a percolation mechanism as the number of layers increased. On ITO, the films were electroactive in acid solution as proved by cyclic voltammetry and they showed fast and reproducible electrochromic transitions.

2.4.1. Pani and GO/Gr in electroactive LbL. A novel completely electrochemical method was presented for the LbL assembly of Pani and graphene sheets.[168] A voltammetric reduction in an aqueous dispersion of both GO and aniline produced the deposition of a Gr layer whereas an oxidative scan in the same solution deposited a Pani layer. The resulting LbL material showed superior conductivity and electroactivity in acid, neutral and also basic solution attributed to the doping effect of Gr on the Pani structure.

In a different approach, sulfonic acid-grafted rGO (by taurine grafting) dispersed in water was assembled with Pani (Rubner-like procedure, pH 3) on APTES-modified ITO electrodes (Fig. 4).[169] The voltammetric response in 0.5 M H_2SO_4 shows the two redox couples of Pani, but the dependence on sweep rate indicates a faster charge transfer in the assembly as compared with Pani, with higher electrical and ionic conductivities, as determined by EIS. The color transitions induced by changes in the applied potential (electrochromic behavior) are also faster and more intense in the assembly.

2.4.2. Pani and GO in LbL sensors. Chemically polymerized Pani was treated as suggested by Rubner *et al.*[61] and assembled by dip-coating with a dispersion of Gr sheets capped with PSS on different PDDA-modified substrates.[170] The films resulted in electroactivity in the pH range 0–8 due to the doping effect of the anionic sulfonates. The stable voltammetric response at pH 7 (−0.6 to 0.6 V *vs.* SCE) shows just a single wave as a consequence of overlapping the redox processes in Pani. The dependence of the voltammetric response on the sweep rate showed no diffusional control, which indicates a fast charge transport within the film. The film-modified ITO electrodes were tested as an amperometric sensor of H_2O_2 at −0.3 V with a linear response on concentration in the sub-millimolar range.

In another work, an aqueous dispersion of Pani (Rubner's method) was employed to form an LbL film on ITO using a hydrazine-reduced GO dispersion as the negative counterpart (Fig. 5).[171] The films were electroactive in neutral solution and the voltammetric current increased with the numbers of bilayers (at least up to 10 bl) due to the doping effect of the carboxylic groups in the graphene sheets. The voltammetric response indicated a surface-confined redox couple and was stable to potential cycling. This promoted the development of

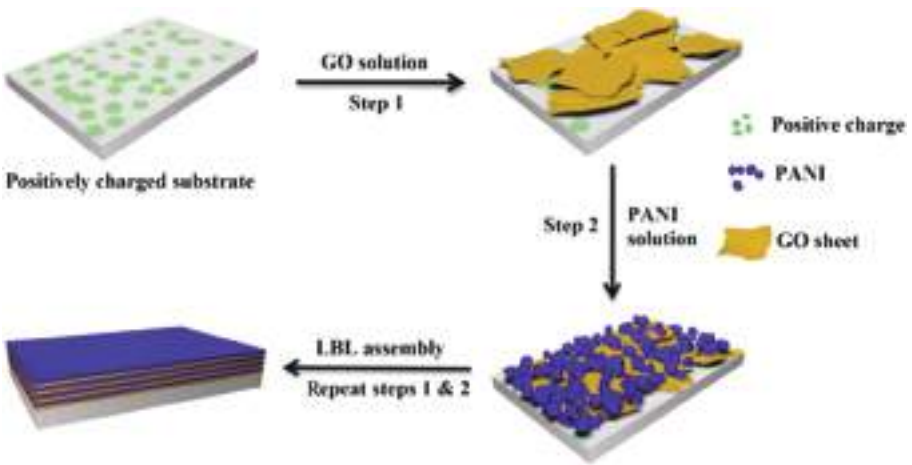

Fig. 3 Schematic representation of the LbL formation of a GO/Pani film on an APTES modified substrate. Reprinted from ref. 167, Copyright (2011) with permission from Elsevier.

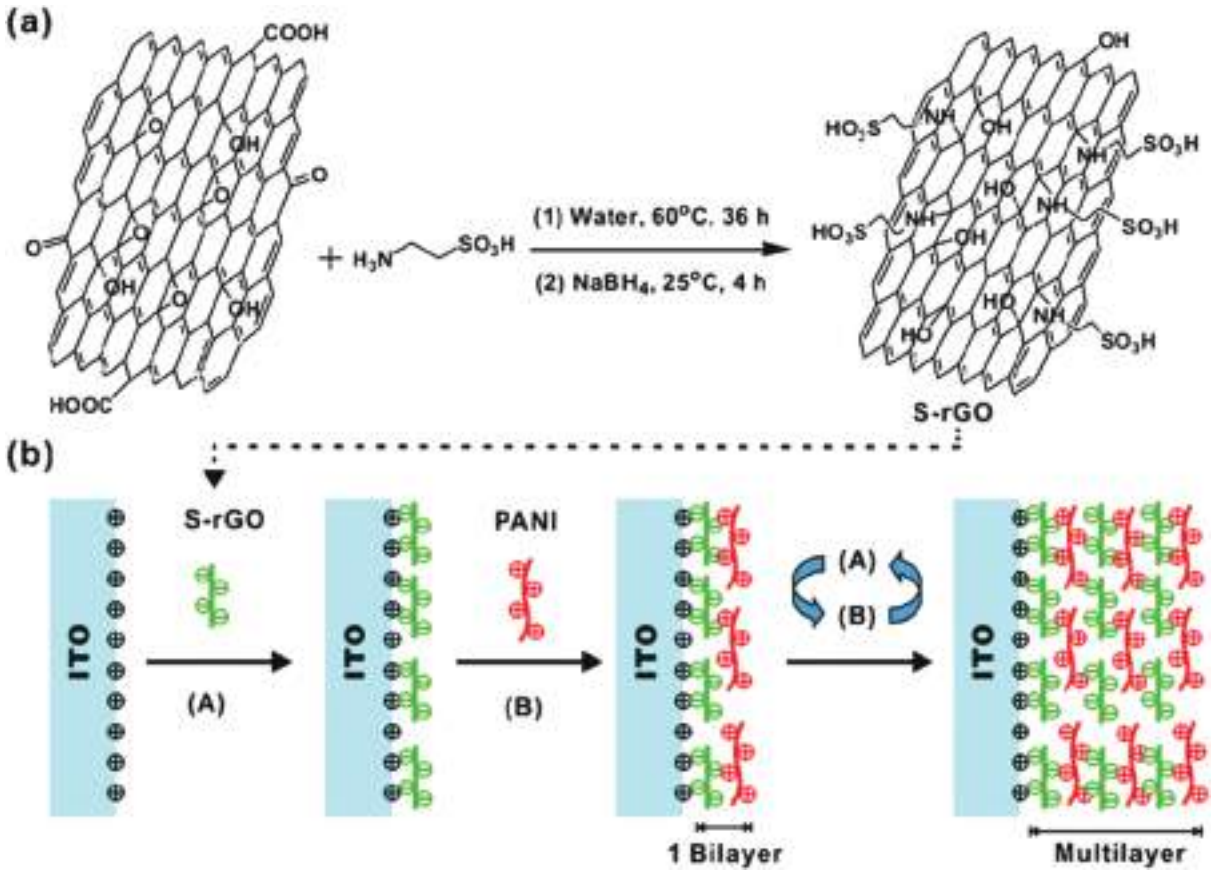

Fig. 4 Schematic representation of the GO modification and LbL assembly with Pani. Reproduced from ref. 169 with permission from the Royal Society of Chemistry.

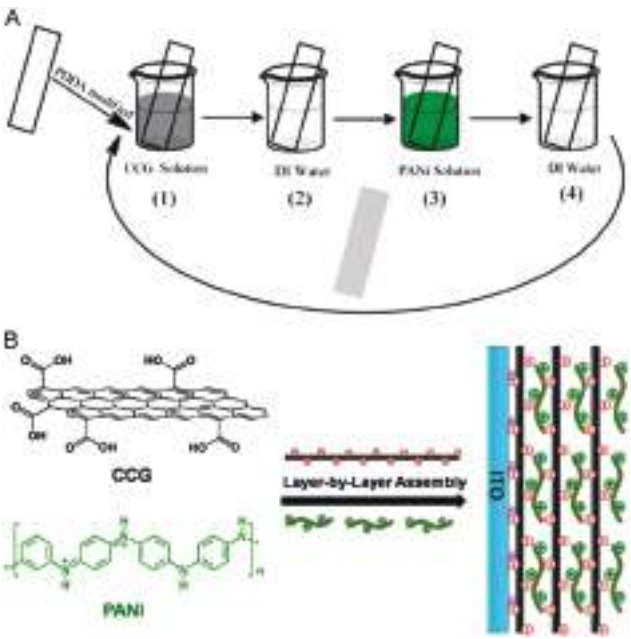

Fig. 5 Schematic representation of dip-coating LbL film formation and the assembly of Pani and chemically converted graphene (CCG). Reprinted from ref. 171, Copyright (2014) with permission from Elsevier.

a voltammetric sensor of ascorbic acid (AA) with a linear dependence of the oxidation voltammetric peak current on the AA concentration (0.1–1.2 mM) in phosphate buffer solution.

In another work, rGO chemically modified by a cationic ionic liquid was assembled with sulfonated Pani by dip-coating.[172] The resulting films show a stable single film-confined quasi-reversible electrochemical response at about 0 V (*vs.* SCE) in neutral PBS, with the voltammetric charge increasing for the successive bilayers. The EIS analysis in the presence of a redox probe indicates a fast electron transfer within the film as a consequence of the synergistic effect of the highly conducting rGO sheets and s-Pani. The voltammetric response in the presence of H_2O_2 showed an increased cathodic current after the polymer reduction peak. The amperometric response at −0.4 V was linear with H_2O_2 concentration (0.5 μM to 2 mM) with a higher response for an optimum number of 8 bilayers.

2.4.3. Supercapacitors and energy devices. Pani from a water dispersion of pH 2.5 (Rubner's method)[61] was assembled with GO (water dispersions of different pH values) by dip-coating on different substrates and then reduced by thermal annealing and vapor chemical treatment with hydrazine.[173] The amount of GO resulted to be smaller as the pH of the dispersions increased as a consequence of its higher negative surface charge. The Pani/Gr multilayers were evaluated by CV

in 1 M H_2SO_4. The two redox couples of Pani were present in a broad capacitive response. The synergistic effect of the high surface area and conductivity of Gr with the redox process in the acidic media of Pani would yield decreased diffusion lengths and fast electron transfer. The specific capacitance and cycling stability per bl decreased from 10 to 40 bl. The chemical reduction with hydrazine led to worse capacitive properties.

In another work, aqueous dispersions of Pani (Rubner's method)[61] and GO of pH 2.6 were employed for dip-coating assembly on ITO.[174] Several reduction methods were assessed, with better results for the use of HI. The electrochemical performance of the modified electrodes was tested in neutral 1 M Na_2SO_4, where they showed a stable response due to the doping effect of the remaining negative groups of rGO on the Pani structure. The capacitive response depended on the GO and Pani concentration in the coating solutions, being the best for the most diluted solutions, where aggregation was avoided.

Gr nanosheets obtained by glucose reduction of dispersed GO were assembled on stainless steel by dip-coating. Then, a layer of Pani nanofibers was electropolymerized by CV in an acidic solution of aniline. By repeating these steps, an LbL film array was formed (Fig. 6).[175] The capacitive behavior of the films was studied in acidic media. The high capacitance was attributed to a combination of the high specific area of the open structure and the pseudocapacitance of redox processes of Pani. The presence of Gr also has an important structural role, as it reduces the decrease of the capacitance during charge/discharge cycling.

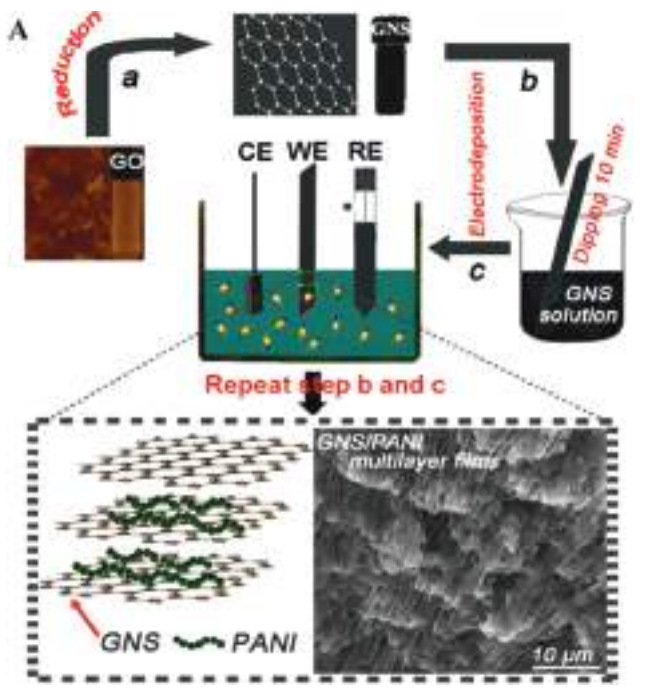

Fig. 6 Schematic representation of the LbL assembly by successive electropolymerization of Pani and dip-coating in graphene nanosheet (GNS) dispersions. Reprinted from ref. 175, Copyright (2013) with permission from Elsevier.

A similar procedure was employed for the construction of LbL films by alternating dip-coating in a GO dispersion and electropolymerization of Pani layers on ITO for high-performance supercapacitors.[176] The films showed better capacitive performance than pure Pani in acidic aqueous solution. The GO offers higher surface areas for polymer anchoring and a synergistic effect was suggested for the electrochemical response.

In another work, aqueous dispersions of Pani of pH 2.6 (Rubner's method)[61] and negatively charged GO were employed for dip-coating assembly on ITO and then Gr was obtained by scanning the potential from 0 to −1.3 V (*vs.* Ag/AgCl) in 1 M H_2SO_4.[174] The films of rGO/Pani displayed high volumetric capacitance, enhanced cycling stability and high charge/discharge rates in acid solution. The superior performance was attributed to a higher degree of reduction of the GO and lower modification of Pani compared to chemical reduction methods.

Similarly, aqueous dispersions of Pani (Rubner's method) and negative GO were employed to grow an LbL film by dip-coating on flexible PET plates.[177] Then, the films were reduced by exposure to HI vapors. The capacitive properties of the film were evaluated in 1 M H_2SO_4. The properties of the assembly resulted in much improvement when it was prepared on an LbL film of poly(*p*-phenylenevinylene)/rGO (PPV/rGO) as the current collector, which also contributed to the increased capacitance providing lesser electrical resistance. The mechanical and potential cycling stability of the double LbL film were excellent due to the presence of the PPV/rGO layers and the hybrid system resulted in being a promising material for the development of flexible microsupercapacitors.

The same procedure was employed for the assembly on FTO.[178] The assembly was electroactive in 0.5 M H_2SO_4, with the typical redox peaks of Pani. The modified electrodes were also evaluated as electrocatalyzers of the I_3^-/I^- redox couple and also as counter electrodes of the dye-sensitized solar cell (DSSC)[179] with I_3^-/I^- as an electrolyte. The electrocatalytic properties were better for higher number of bilayers in the LbL and it would be due to a higher real interfacial area and low charge transfer resistance. The same effect was observed for the photon-to-electron conversion efficiency in the DSSC.

In a similar approach, dispersions of complexes of Pani and SWNTs were LbL assembled with negative GO on FTO (Fig. 7).[180] The modified electrodes were tested for the electroreduction of I_3^-/I^- in acetonitrile. Both, voltammetric and EIS results indicate an increase in the performance as the number of bilayers increases, due to the incremental number of bondings between Pani and SWNTs, which would allow rapid electron transfer as well as the high active specific area of the assemblies. Finally, the films were employed as counter electrodes in the DSSC and the conversion efficiency resulted in being dependent on the number of bilayers and the SWNT dosage.

More recently, Pani-grafted CNTs were assembled LbL with Pt NPs to be employed in the DSSC by dip-coating on FTO electrodes.[181] The grafting was obtained after chemical oxidation of the aniline bound to GO by reflux complexation. The films were tested as cathodes in the DSSC for the electro-reduction

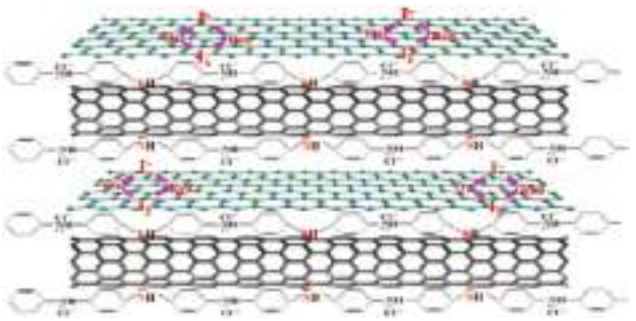

Fig. 7 LbL assembly of Pani-capped SWNTs and GO sheets for the dye-sensitized solar cell. Reprinted from ref. 180, Copyright (2014) with permission from Elsevier.

of I_3^- in aqueous solution. The increasing number of bilayers not only produced higher electroactive areas but also diminished the charge resistance producing higher electron transfer rates.

In a totally different approach, PSS-rGO sheets and chemically polymerized Pani were assembled on polystyrene microspheres.[182] Then the polystyrene was dissolved to obtain hollow microspheres and drop-cast on a glassy carbon electrode (Fig. 8). The films were tested for being employed in supercapacitors. The voltammetric response in 1 M H_2SO_4 corresponds to a surface confined couple with the typical peak of Pani, with an optimum response for the film of 6 bilayers. The structure of the cast film presents a high specific area which highly increases the number of electroactive sites. The charge/discharge curves show a non-triangular shape, which indicates a combination of double-layer (DL) capacitance and pseudocapacitance and the specific capacitance is superior to that of the LbL film grown on a plane substrate.

In another work, Pani nanofibers and GO were assembled by dip-coating from aqueous dispersions.[183] The results of QCM indicate that the films are mainly composed of Pani, whereas SEM results show that there is no clear stratification

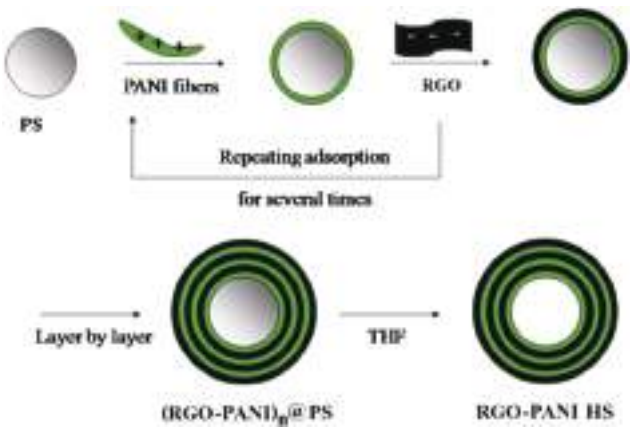

Fig. 8 Construction of hollow spheres by LbL assembly of PSS-RGO and Pani. Reprinted from ref. 182, Copyright (2015) with permission from Elsevier.

and a porous structure (confirmed by void fraction calculation), and patchy deposition is suggested. The modified electrodes were then electrochemically reduced at 1.5 V *vs.* Li/Li^+ in 0.5 M $LiClO_4$ in propylene carbonate. This assembly is much more stable to oxidation than similar ones probably due to the interaction between Pani and the oxygen-containing groups of the rGO. Current limitations due to hindered ion movements were observed for the thicker films. Galvanostatic charge/discharge curves in this organic electrolyte reveal a high specific capacity that would be due to a faradaic contribution of Pani and oxygen-containing groups of rGO and a double layer-type which is enhanced by the highly specific area of the conductive material/solution interface. The electrodes also present excellent cycling stability compared to Pani films under the same conditions.

In a different approach, the LbL assembly of Pani nanofibers and GO on ITO was achieved by spray-assisted LbL from aqueous solutions.[184] The films were electrochemically reduced in an organic solution (0.5 M $LiClO_4$ in propylene carbonate) and tested in Li-ion cells. The film showed two redox peaks at about 3 and 3.4 V *vs.* Li/Li^+ corresponding to the transitions in Pani. The voltammograms show ion transport limitations only for very thick films (more than 100 bl) owing to the very porous structure. These modified electrodes presented a superior capacitive performance as compared to dip-coated produced LbL assemblies, which was attributed mainly to the higher void fraction. Additionally, the method of spray-assisted LbL is more adequate for large-scale production than the traditional dip-coating method.

Additionally, an LbL vacuum filtration method was employed to assemble Pani-functionalized rGO and electrochemically exfoliated Gr (EGr) on PTFE membranes and then dry-transferred to other substrates (Fig. 9).[185] The result is an alternation of thin layers (10–20 nm) of EGr and thick layers (2 μm) of Pani-rGO, yielding a mesoporous structure accessible to ions in solution. The electrodes presented a high areal and volumetric capacitance, with a capacitive performance superior to electrodes without layered stratification. The EGr layers serve as both DL and pseudocapacitive capacitors, and would provide an elastic spatial confinement for the Pani layers allowing the mechanical changes coupled to the redox transformations but maintaining the whole system integrity. The electrodes were tested as all-solid-state microsupercapacitors with an in-plane interdigital design with PVA/H_2SO_4 as the electrolyte, which showed a good capacitive performance even on flexible PET substrates. Arrays of these MSCs were employed as real power sources of LEDs enhancing their practical utility.

3. Structural and functional characterization of the assemblies

3.1. UV-visible characterization

3.1.1. Electronic transitions in Pani. Pani based materials show intense electrochromism due to the changes of the electronic structure on the oxidation degree (applied potential).

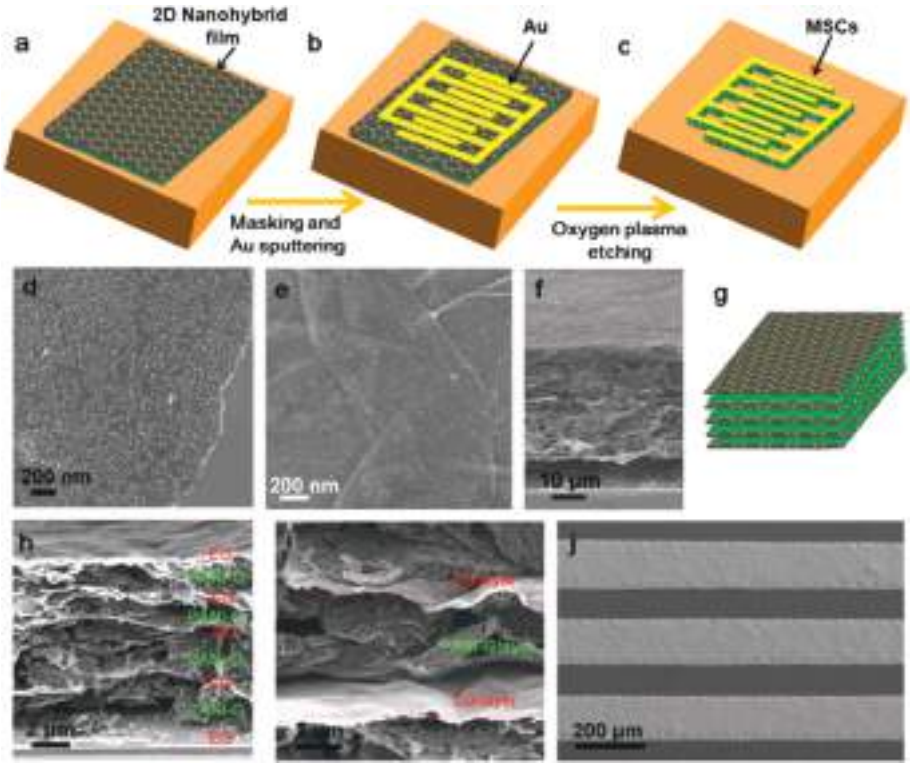

Fig. 9 Construction of the micro-supercapacitors (MSCs) of stacked Pani, graphene and SEM images of the assemblies. Reproduced with permission from ref. 185 Copyright 2015 Wiley-VCH Verlag GmbH & Co. KGaA, Weinheim.

Several studies describing electronic transitions in Pani have been published in the last 30 years. Here, we just offer a short review of the most important features of Pani film bands in the UV-visible range.

In the case of the reduced form of Pani (LB), the electronic transitions are only observed below 350 nm. The bands below 300 nm and approximately 325 nm are assigned to π–π* transitions of the benzenic rings distorted by the presence of amino groups.[38,186–189] These transitions are associated with the band-gap of the material in the reduced state.[190,191] By protonation, the auxochromic effect of the amino group diminishes, shifting the transition to shorter wavelengths as a consequence of the increase of the band-gap.[41,191]

The basic form of emeraldine (EB) also presents a band at 320 nm, but another band appears at about 600 nm corresponding to the exciton state of quinoid rings. The excitonic transition comes from an interchain absorption that leads to a separate charge state (molecular exciton) with a positive charge on a benzenic unit and a negative charge on a quinoid one.[38,190,191] As this transition arises from the HOMO of benzenic to the LUMO of the quinoid ring, it is sometimes indicated as (π_B–π_Q).[192] After protonation, the band of ES shifts from 600 to 800 nm due to the transition from quinoid units to the semi-quinoid ones (polarons) extended all over the chain.[191] This band has been named as (π_B–π_R) indicating the excitation from the valence to the polaron band formed within the gap.[191] The valence band loses electrons from the benzenic rings and shifts upper in the gap forming the polaronic band. This phenomenon is consistent with the conformational distortion that induces a new transition at about 400–450 nm from the low valence levels to the polaron band.[193]

Finally, the completely oxidized form of Pani (PB) shows a band at about 350 nm associated with the band-gap (π–π*) transition of the quinoid rings[194,195] and another band at 540 nm assigned to the excitonic transition. After protonation, the first band shifts to 300 nm as another intense band appears at 620 nm. Albuquerque *et al.* have deconvoluted this band as two Gaussians, one associated with the molecular exciton and the other with the *Peierls gap*. The first contribution is that observed in EB and LB, while the other just appears in PB.[38,196]

3.1.2. UV-visible transitions in carbon nanomaterials. In the case of SWNTs, several absorption bands in the near-IR are assigned to DOS transitions, but only one band appears in the UV-visible region, assigned to π-plasmon transitions at about 275 nm.[197] On the other hand, graphene presents an extended π system that allows absorption over the entire UV-visible range. Strictly, Gr is a zero-band-gap semiconductor and conduction is possible by thermally excited electrons.[198] However, the decrease of symmetry generates an increase in the band-gap, as happens in the case of oxidation or stacking of Gr layers.[199] In this sense, GO can be considered as a hybrid material that presents conducting π-states from the sp^2 carbon atoms and an energy gap owing to the sp^3 carbon atoms.[200]

The oxidation degree determines the proportion of sp^2 and sp^3 atoms and, hence, the band-gap energy. Associated with the band-gap, there is the possibility of a band-gap transition (π–π^*) in the GO, which typically requires UV radiation.[201] The increase of sp^2 carbons in rGO diminishes the band-gap energy and shifts the π–π^* transition to higher wavelengths. In the case of GO, a shoulder at about 360 nm assigned to (n–π^*) transitions of the carbonyl groups has also been reported.[201]

3.1.3. Electronic transitions in the LbL assemblies. UV-visible spectroscopy is a simple, rapid and inexpensive method that allows monitoring the growing of LbL assemblies when some of the components feature electronic transitions in this spectral range (Fig. 10). Pani-based polymers are colored owing to several electronic transitions in benzenic, polaronic and bipolaronic structures. Consequently, the absorbance of these bands has been extensively employed to monitor the growing of LbL films. Even in the initial studies on LbL assembly of Pani, a quantitative evaluation of the amount of polymer by employing the absorption coefficient of the excitonic band for the dedoped Pani was presented.[61] From then on several bands have been reported to linearly increase with the number of deposition cycles, as summarized in Table 1 for the LbL assemblies with the carbon nanomaterials reported here.

On the other hand, the appearance of a band at about 270–290 nm has been reported to be caused by the incorporation of MWNTs to Pani in different composites.[202–204] Also, a new band at about 520 nm has been assigned to the interaction of imine groups with anionic groups in carboxylated MWNTs.[204]

Table 1 UV-visible bands and assignments for the LbL films of Pani and carbon nanomaterials in this article. Bold numbers indicate the wavelength at which a linear dependence of the absorbance on the deposition cycles was reported

Pani	Carbon nanomaterials
325 nm (π–π^*), 650 nm (excitonic π_B–π_Q of EB)	259 nm (s-MWNTs)[113]
320 nm (π–π^*), **630** nm (excitonic π_B–π_Q of EB)	280 nm (rGO)[167]
319 nm (π–π^*), 458 nm (polaron)	220 nm (GO); 275 nm (rGO)[173]
310 nm (π–π^*), **880** nm (π_B–π_R of ES)	280 nm (rGO)[174,177,206]
339 nm (π–π^*), **445** nm (polaron)	**220** nm (PSS in PSS-rGO)[170]
560 nm (excitonic π_B–π_Q of EB) (s-Pani)	**270** nm (IL-rGO)[172]
440–447 nm (polaron), **900** nm (π_B–π_R of ES)	231 nm (GO)[178,180]
339 nm (π–π^*), **665** nm (excitonic π_B–π_Q of EB)	231 nm (GO); **270** nm (rGO)[171]

As a consequence of the reduction of GO, the band at about 220–230 nm shifts to high wavelengths (270–280 nm) owing to the increased conjugation extension (lower band-gap) and the absorption in the whole visible range also increases.[167,171] Thus, the samples of GO get darker after reduction, which indicates the restoration of the π extended system (Fig. 11).[171,174,177,205]

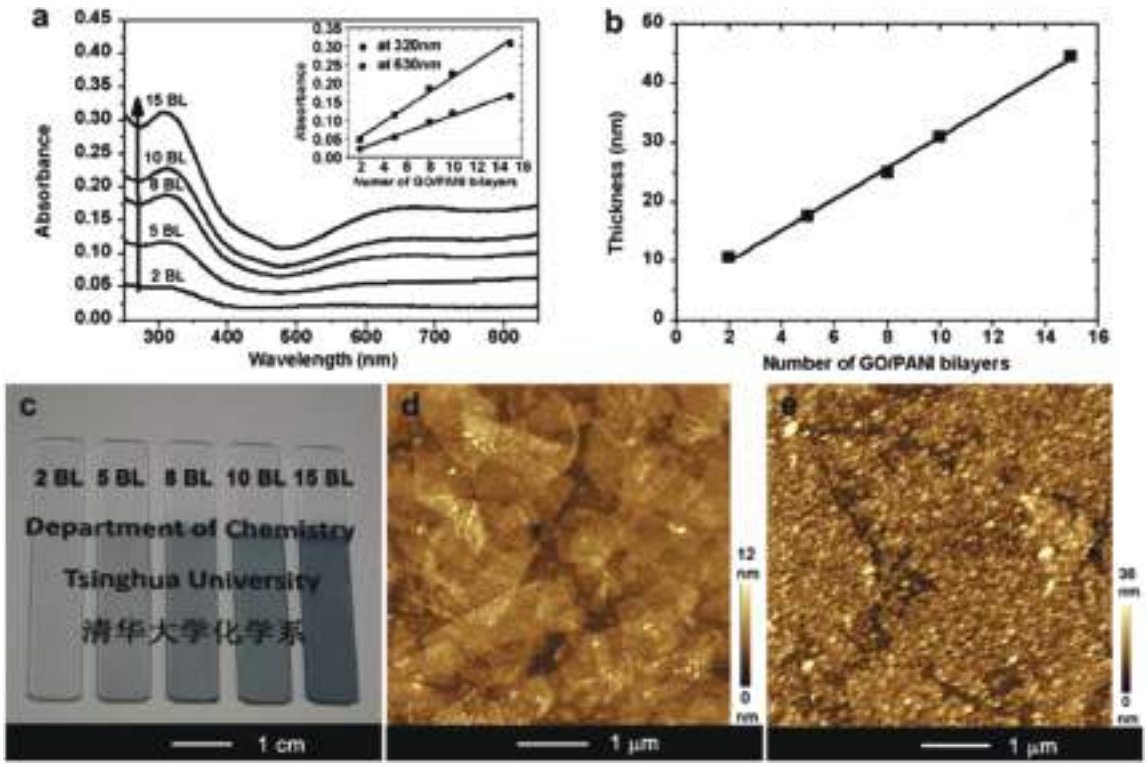

Fig. 10 (a) UV-visible spectra of GO/Pani LbL assemblies on quartz slides (c); thickness (b) and AFM images (d, e) of the films. Reprinted from ref. 167, Copyright (2011) with permission from Elsevier.

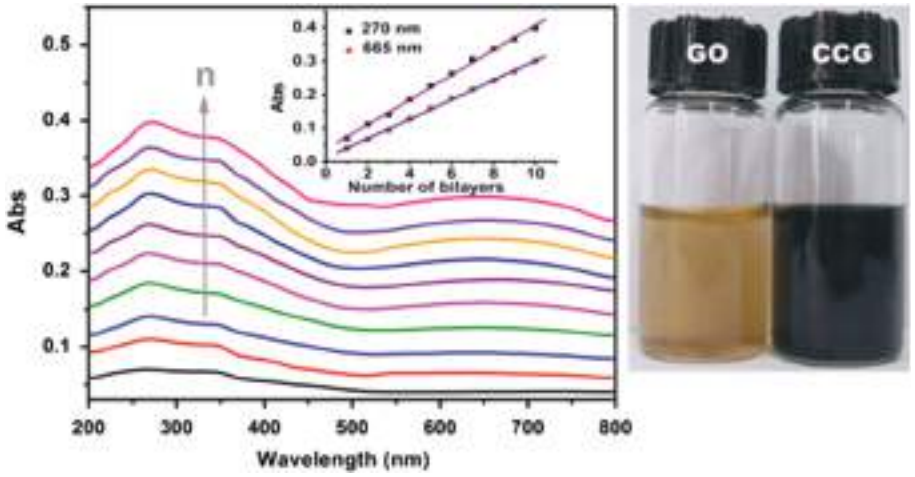

Fig. 11 UV-visible spectra of LbL films of Pani and chemically converted graphene (CCG) and pictures of GO and CCG dispersions. Adapted from ref. 171, Copyright (2014) with permission from Elsevier.

3.2. Thickness and electronic conductivity

Most studies report a linear increase of the amount of the deposited material with the number of deposition cycles. The thickness, and more precisely the thickness per bilayer, is a critical parameter of the LbL assemblies as it strongly affects the degree of control of the material organization at the molecular level, but also the steps and time required to obtain a given film. Several techniques have been used to determine the thickness in the LbL films of Pani as summarized in Table 2. The values of previous studies by Rubner's group with polyelectrolytes were included for comparison.[61,62] Although there is some dispersion of the values (7 ± 6 nm bl^{-1}), the application of the dip-coating method for carbon nanomaterials yields thicknesses similar to those obtained when polymers are used as counterparts in the Pani-containing LbL films. However, this not necessarily implies an ordered succession of uniform layers.

The sheet resistance characterizes the in-plane electronic conductivity of thin films and it is equivalent to the bulk resistivity divided by the film thickness. It is commonly expressed in ohms per square (Ω sq^{-1}) and it is directly measured by the four-probes method.[207] Sheet resistances of some Pani-containing LbL films are reported in Table 3. The measure of the conductivity of the Pani/rGO films shows that a minimum number of layers is needed to obtain the limiting value of the sheet resistance.[167,174] This suggests that there is a percolation of the carbon nanomaterials during the assembly. Moreover, it is found that the conductivity of the assemblies is controlled by the CNTs if its proportion in the composite exceeds a percolation limit.[131] On the other hand, the roughness determined by AFM increases with the number of deposition cycles[117,135] and the root-mean-squared roughness values indicate the assembly of Pani grains[167] or fibers yielding highly entangled porous films.[135] However, the roughness has been reported to decrease by thermal treatment of the Pani/CNT films[135,173] or reduction of the Pani/GO[206] films, which also enhances the mechanical stability. In the case of Pani fibers, the thickness per bilayer is lower than the fiber diameter which indicates that the films are formed by patchy adsorption.[183] The same fact had been found in the assembly of Pani with polyelectrolytes, for which a minimum number of deposition cycles was

Table 2 Thickness of the different Pani-containing LbL assemblies in this article

LbL	Assembly method	Thickness (nm/bilayer)	Technique
Pani/PSS[61]	Dip-coating	1.2–3.6	Profilometry
Pani/non-ionic polymers[62]	Dip-coating	5–12	Profilometry
Pani/MWNTs[114]	Dip-coating	6	Ellipsometry
Pani/MWNTs[124]	Dip-coating	1.8	SPR + simulation
Pani/MWNTs[135]	Dip-coating	13	Profilometry
Pani/PSS-MWNTs[117]	Dip-coating	9	AFM
Pani/rGO[167]	Dip-coating	3	AFM
Pani/GO[173]	Dip-coating	19	Ellipsometry
Pani/S-rGO[169]	Dip-coating	4.8	Profilometry
Pani/GO[174,206]	Dip-coating	2.4	Ellipsometry
Pani/PSS-GO[170]	Dip-coating	14	Profilometry
Pani/rGO[177]	Dip-coating	2.24	Ellipsometry
Pani/GO[183]	Dip-coating	9.6–4.4	Profilometry
Pani/GO[184]	Spray-assisted LbL	46	Profilometry
Pani/MWNTs[131]	Spray-assisted LbL	169	SEM

Table 3 Sheet resistances of some Pani-containing LbL assemblies in this article

LbL	Sheet resistance
Pani/SWNT[131]	20 kΩ sq^{-1}
Pani/rGO[167]	106 to 6 kΩ sq^{-1} (2 to 15 bl)
Pani/rGO[174]	$2{\cdot}10^5$ to 5.3 kΩ sq^{-1} (1 to 15 bl)
Pani/rGO[177]	2.2 kΩ sq^{-1} (53 bl)

required to obtain conductivity values similar to the bulk ones.[61] This reinforces the idea that several layers are needed to produce a fully continuous film with a percolation of the conducting components.

Although a certain degree of stratification of the Pani/CNT films inferred from the conductivity anisotropy has been reported,[114] the general case is that non-uninform deposition of discrete layers can be achieved by dip-coating.[170] Contrarily, in the spray-assisted assemblies a notable stratification can be achieved, which is mainly owing to the higher amount of material deposited in each layer,[184] (Fig. 12) yielding thicker bilayers as shown in Table 2.

3.3. Raman spectroscopy

Raman spectroscopy is a powerful tool for the study of carbon materials as it provides structural and electronic information and it is also a rapid and non-destructive technique.[208] Due to their particular electronic structure, both CNTs and graphitic compounds show no band-gap which generates a resonance condition with all wavelengths of the incident radiation.[208,209] This resonance notably increases the intensity of the Raman lines and allows the study of small samples up to Gr monolayers.

The main Raman peaks of graphitic materials are those called G and D bands. The G band corresponds to the high frequency E_{2g} phonons.[208] It is an in-plane vibration that compresses the graphene sheets. It appears at about 1590 cm^{-1} but its position depends on the number of layers[210] and also on the state of strain,[211] doping[212] and temperature.[213] On the other hand, the D band is due to the breathing mode of the six atom ring and it becomes Raman active just when certain defects in the structure are present.[208] It appears at about 1350 cm^{-1}, but as it is a dispersive band, its position depends on the excitation energy.[208] The intensity of this band is related to the number of defects or edges of the carbon material and the ratio $I(D)/I(G)$ can be employed as a measure of the disorder.[208] Both G and D bands reported in this article for the carbon nanomaterials employed for the LbL with Pani are summarized in Table 4.

3.3.1. Raman of Pani and assemblies. Several studies describe the Raman band assignments for different redox states of Pani.[214–218] The main features appear in the range 1000–1700 cm^{-1}. The C–H in-plane bending modes appear at about 1160 and 1190 cm^{-1} for quinoid and benzenic units respectively.[215] Particularly, the bands assigned to the CN

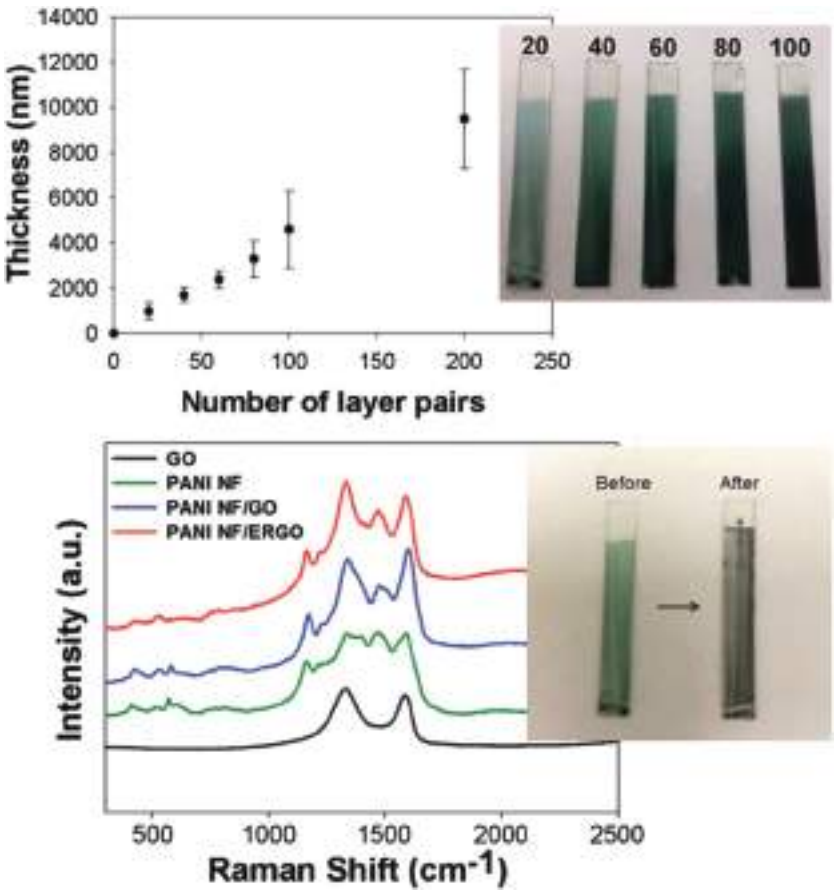

Fig. 12 Thickness determined by profilometry of the spray-assisted LbL films of Pani nanofibers and GO of different numbers of bilayers (pictures) (top). Raman spectra of single components and assembled films before and after the electrochemical reduction (pictures) (bottom). Adapted from ref. 184 with permission from the Royal Society of Chemistry.

Table 4 Band positions for carbon nanomaterial components of Pani/nanomaterial LbL assemblies

Sample	D band/cm^{-1}	G band/cm^{-1}	λ/nm
GO[174]	1343	1596	633
GO[206]	1343	1600	633
GO[183]	1335	1590	514
GO[184]	1330	1580	514
IL-rGO[172]	1355	1580	514
MWNTs[115]	1350	1585	514
MWNTs[132]	1326	1574	633
MWNTs[135]	1355	1580	785
PSS-rGO[182]	1358	1582	514
PSS-rGO[170]	1355	1580	514
rGO[174]	1336	1587	633
rGO[206]	1332	1583	633
rGO[168]	1301	1595	633
rGO[171]	1319	1587	514

stretching appear at different wavelengths depending on the redox and doping state: 1220–1270 cm^{-1} (amine in LB, LS); 1310–1400 cm^{-1} (radical cation, ES), 1470–1490 cm^{-1} (quinone diimine, EB).[214] The CC stretching modes also appear in this region: the C–C stretching of the E form appears at about 1500 cm^{-1} (EB) and 1620–1630 cm^{-1} (ES);[215,219] the C=C stretching of the Q units is at about 1570–1595 cm^{-1},[218,219] whereas the C–C stretching of Q units appears at about 1420 cm^{-1} (EB).[218]

The Raman peaks reported in LbL assemblies are summarized in Table 5 together with the assignment informed in each work.

In the case of Pani/carbon nanomaterial LbL assemblies, the peaks of Pani are so intense that in most cases no peaks owing to the carbon nanomaterials can be observed.[132] Nevertheless, the analysis of the intensity ratio I(D)/I(G) can be employed to evaluate the efficiency of the reduction treatment of GO in the assemblies (Fig. 12).[174,206]

On the other hand, in some cases, it is possible to infer some structural information from the changes in Pani bands in the presence of the nanomaterial. The position of the C–N$^+$ stretching band has been reported to be sensitive to the interaction with anionic groups and also the relative intensity ratio of these bands to the C–H bending band increases with the doping level.[220]

3.4. X-Ray characterization

3.4.1. X-ray diffraction (XRD). X-ray diffraction allows determining the presence of domains of crystallinity or ordered structures in the samples. Sometimes it is also possible to identify crystalline phases or to determine the characteristic distance of a given array. In the case of Pani/carbon nanomaterial LbL assemblies, this technique can provide further information about the structure of both components. Most studies are performed with a Cu-Kα radiation source, so the results can be compared in both the diffraction angle (2θ) and characteristic distance (d).

Dedoped Pani only shows a broad diffraction peak at about 19 degrees, but acid doped Pani presents a series of peaks at about 9, 15, 22 and 26 degrees indicating a certain degree of crystalline domains.[221,222] The characteristic peak of the Bragg diffraction at 2θ = 26.1 degrees corresponding to the interlayer spacing of the cylindrical graphite nanotubes (d = 0.34 nm) is also present in the XRD pattern of the Pani/sMWNT LbL assembly, together with weak broad peaks attributable to doped Pani at about 26 and 22 degrees (d = 0.34 and 0.4 nm).[113] In another case, the composites of Pani and MWNTs show Bragg peaks at 2θ = 15, 22 and 26 degrees attributed to Pani but also two peaks around 26 and 43 degrees corresponding to the interlayer spacing of the nanotube (d_{002}) and the d_{100} reflection of the carbon atoms, respectively.[223]

During the exfoliation of graphite to produce GO, there is a transition between two clear diffraction peaks. The typical diffraction peak of pristine graphite is observed at about 2θ = 26° (d = 0.34 nm) whereas a diffraction peak at about 2θ = 10–12.1° (d = 0.73–0.86 nm) appears after oxidation due to the introduction of oxygen-containing functional groups on the graphite sheets.[201,224] When the exfoliation is completed, no diffraction peaks are observed owing to the absence of staking.[224] It has also been reported that the sheet spacing slightly increases with the oxidation degree of the GO between 0.8 and 0.95 nm.[58] After reduction of the GO, the XRD pattern

Table 5 Band positions (cm^{-1}) for the Pani components of Pani/nanomaterial LbL assemblies. Q = quinoid unit; B = benzoid unit; EB = emeraldine base; ES = emeraldine salt

Pani/assembly	λ/nm	CH in-plane bending	Radical C–N$^+$ stretching	C=NH$^+$ (ES), C=N (EB), stretching	C=C quinoid stretching
Pani(MWNTs) (ES)[132]	633	1171	1330	1504	1593
Pani(MWNTs) (ES)[220]	514	1176	1332	1489	1580
Pani-MWNTs[135]	785	1166	1338	1484	1580
Acid doped Pani (ES)[168]	633	1182	1320–1377	1512	1599
Reduced (PANI/GO)[174]	633	1156	—	1509	—
e-rGO/Pani (EB)[206]	633	1156	—	1455	1405(C–C)
Pani (EB)[170]	514	1166	—	1486	1580
s-Pani (EB)[172]	514	1166	—	1486	1580
Pani (ES)[171]	514	1169	—	1475	1596
Pani/PSS-rGO (EB)[182]	514	1166	—	1486	1580
Pani nanofibers[183]	514	1158	1330–1440	1480	1580
Pani nanofibers/(e-rGO)[184]	514	1166	1386	1486	1580

changes again and a broad peak at about 23–25 degrees appears indicating that the interlayer distance is slightly higher than in graphite.[201]

After reduction by glucose, the peak at about 2θ = 12 has been reported to disappear and a new peak appears at 2θ = 24.6 degrees.[175] The interlayer spacing, slightly higher than that of graphite, indicates some remaining oxidation and the broadness of the peak suggests the presence of a few loosely stacked layers. The XRD patterns of pristine Pani and the electrochemically produced LbL Pani/rGO composite present almost the same peaks, with a little higher intensity in the last case, indicating that the presence of rGO induces higher crystallinity in the conducting polymer. The peaks of rGO are overlapped by those of Pani (Fig. 13).[175]

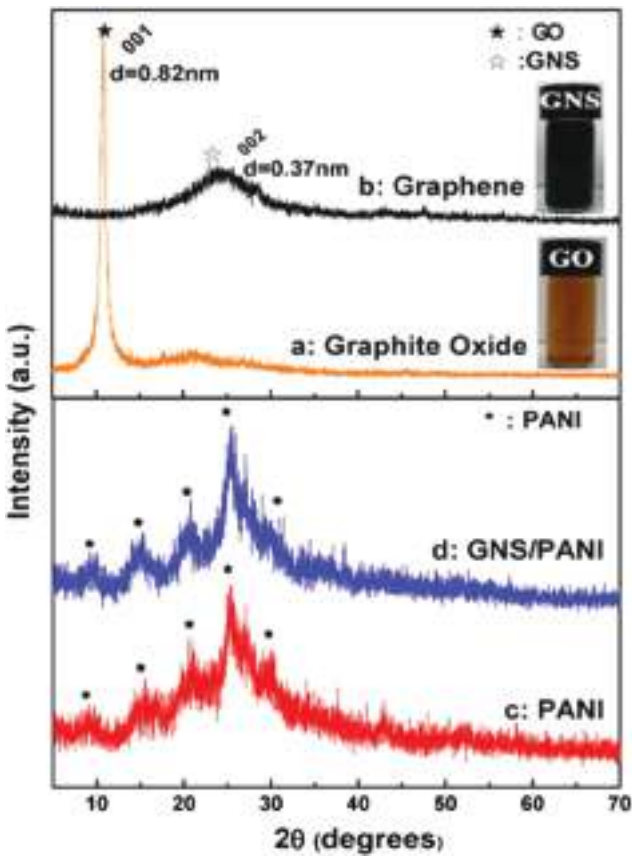

Fig. 13 XRD patterns of GO, graphene nanosheets (GNS), Pani and the composite. Reprinted from ref. 175, Copyright (2013) with permission from Elsevier.

A similar change was observed for the reduction of GO by an ionic liquid that transforms the sharp peak at 2θ = 9.2 degrees into a broad peak at 2θ = 24.5 for the IL-rGO.[172] Furthermore, in another study, the peak of GO at 2θ = 11.5 degrees turns into a broad peak at 2θ = 23.6 degrees after reduction with hydrazine.[171] This peak and those of Pani are overlapped in the XRD pattern of the LbL assembly.

3.4.2. X-ray photoelectron spectroscopy (XPS). X-ray photoelectron spectroscopy allows the determination of surface atomic composition and chemical state of each element (speciation), which is extremely important information for the characterization of film-modified surfaces. The N 1s core level peak is caused mainly by Pani whereas the C 1s signal is usually employed for the characterization of the carbon nanomaterials.

The N 1s core spectrum level of Pani can be deconvoluted into 4 components.[225] The component of lower BE, at about 398.5 eV, has been attributed to the neutral N of the imine moiety (=N–).[226–229] The component at about 1 eV higher BE has been assigned to the neutral backbone or terminal amine (–NH–/–NH_2).[227,229] Charged nitrogen species are expected to appear at higher BE than the neutral ones, so the components at about 400.6 and 402.1 eV have been usually referred as positive nitrogen species and sometimes are fitted as a single component at about 401 eV (N^+).[227–230] The component at about 400.6 eV has been assigned to oxidized secondary amines (delocalized polaron-type structure, sometimes called radical cations) whereas the other peak at about 402 eV would be due to protonated imine (localized bipolaron-type structure).[227,229] The assignments of the components at the N 1s core level of the XPS peaks of Pani-containing LbL assemblies are summarized in Table 6. In the presence of oxidized SWNTs, the relative contribution of protonated to neutral imines increases, which suggest stabilizing interactions of protonated groups of Pani with the carboxylates of the CNTs.[114] A higher doping degree was also confirmed by XPS in the case of Pani/rGO owing to the presence of graphene nanosheets.[175] Even the electrochemical reduction of Pani/GO in acidic media was also reported to produce an increase in the doping level as suggested by the higher proportion of quinoid and positive nitrogen species.[206]

The C 1s core level of CNTs can be deconvoluted in several components (Table 7). The main component in pristine CNTs

Table 6 Assignment and BE of the N 1s components of Pani in LbL assemblies and films

LbL assembly	=N-neutral imine	–NH–/–NH_2 neutral amines	–NH^+-polaron structure	=NH^+-protonated imine	Internal reference
Pani film[225]	398.5 eV	399.6 eV	400.6 eV	402.1 eV	C 1s (CC/CH) at 285 eV
Pani/SWNT-COO^- [114]	398.9 eV	399.8 eV	400.6 eV	402.0 eV	C 1s (sp^2) at 284.7 eV
Pani/MWNT[135]	398.2 eV	399.9 eV	401.1 eV (N+)		C 1s (sp^2) at 284.5 eV
Pani/GO[173]	398.2 eV	399.4 eV	401.1 eV (N+)		C 1s (sp^2) at 284.4 eV
Pani/rGO[175]	398.2 eV	399.4 eV	401 eV (N+)		C 1s (sp^2) at 284.5 eV
Pani/GO[206]	397.5 eV	298.9 eV	401 eV (N+)		C 1s (sp^2) at 284.5 eV

Table 7 Assignment and position (BE in eV) of the C 1s components in carbon nanomaterials and some assemblies with Pani in this article

Sample	Graphitic C sp^2 (*)	CH/sp^3 C	CN	C–OH, –C–O–	–C═O	COOH
COOH-SWNT[116]	284.5	285.1		286.2	287.5	288.9
Pani/GO[173]	284.4	285.1	285.8	286.6	288.0	289.9
Taurine-rGO[169]	284.5		286.5	286.0, 286.7	287.7	289.5
Pani/GO[206]	283.5			286.0	287.8	289.5
Pani/e-rGO[183]	284.5		285.1	285.8, 286.7	287.3	288.6

(*) used as internal reference.

is assigned to the sp^2 C of the graphitic structure that is similar to the asymmetric peak of graphite (284.66 eV).[231,232] This peak is usually employed as an internal reference for the entire XPS signal of graphitic-like materials and stated to be at about 284.5 eV.[231,233] There is another peak with higher BE assigned to diamond-like sp^3 carbon atoms, which is related to the presence of defects in the tubular structure of the CNTs[232] and increases upon oxidation.[231] Then, there are several components caused by the presence of oxygen in different functional groups. The BE of these peaks increases with the oxidation degree of the C atoms: carbons of ether, epoxy and hydroxyl moieties (–C–O–) appear at about 286.5 eV, whereas carbonylic (–C═O) and carboxylic (COOH) carbons appear at about 288 and 289 eV respectively.[231–233] Finally, there is another peak at higher BE (290.5–291.5 eV) assigned to a π–π* transition loss peak (shake-up structure).[232,233] In the case of GO, the assignments of the C 1s components are similar. The sp^2 C component was reported to be at 284.4–285.1 eV and the oxygen-containing functionalities with chemical shifts of 1.3–2.3 for (–C–O–), 2.7–3.6 for (–C═O) and 3.8–4.7 for (COOH).[201,234,235] After reduction with hydrazine, also a component assigned to (–CN–) close to that of (–C–O–)

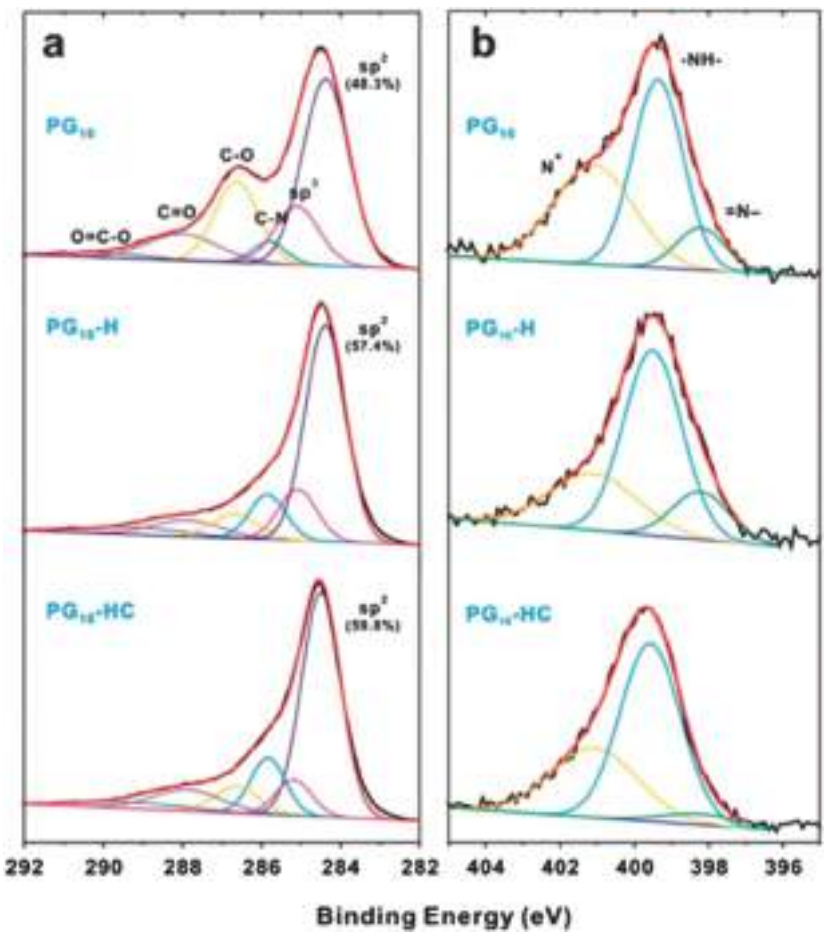

Fig. 14 XPS spectra of (a) C 1s and (b) N 1s core levels of an LbL Pani/GO film (10 bl) as prepared and after heat treatment (H) and heat and chemical treatment (HC). Reproduced from ref. 173 with permission from the Royal Society of Chemistry.

has been reported.[234] Additional components owing to C bound to N are also expected in the presence of Pani. Chemical shifts of 0.6–0.9 and 1.4–1.9 eV relative to the internal reference (CH/CC) have been reported for uncharged (–CN–) and charged (CN+/C=N+) nitrogen-containing functionalities of Pani respectively.[227,229]

The C 1s core region has been extensively employed to study the reduction of GO previous to the assembly or within the LbL films. In this sense, an increase of the sp^2 C 1s signal and a decrease of the oxygen-containing components have been reported by reduction with taurine. The presence of a new component of CN and peaks for N 1s and S 2p in the survey indicates that taurine is effectively grafted.[169] Moreover, most of the carbonylic components (–C=O) of the C 1s signal of GO disappeared after reduction with glucose.[175] The same has been observed after electrochemical reduction in acidic aqueous solution, which produces a decrease of the oxygen-containing components even higher than the treatment with HI.[206] A similar decrease of the oxidized moieties has been observed after electrochemical reduction of the Pani/GO assemblies in organic electrolyte.[183] Furthermore, the proportion of the graphitic sp^2 C 1s signal has been reported to increase after chemical and thermal reduction of the Pani/GO films with a concomitant decrease of the radical cationic nitrogen component (N+) in the N 1s core level (Fig. 14).[173]

3.5. Electrochemical characterization

3.5.1. Cyclic voltammetry. Cyclic voltammetry is a very popular electrochemical technique that has been extensively employed for the study of electroactive films.[236] It provides information about the amount of electroactive material, redox potentials and the electronic and ionic charge transport.[25] For thin films and fast electronic and ionic charge transport, the voltammetric response is reversible (quasi-equilibrium).[237] Under these conditions, the peak current is proportional to the sweep potential rate and the voltammetric integrated charge is proportional to the amount of connected electroactive material.[25] On the contrary, if the charge transport within the film or the charge transport at the interfaces is slow, the voltammetric response becomes diffusional or quasi-reversible. In the particular case of diffusion limited charge transport, the peak current linearly increases with the square root of the sweep rate and the effective (electronic, ionic or mixed) diffusion coefficient can be obtained.[25,236] On the other hand, in the case of quasi-reversible processes, the voltammetric peaks shifts with the sweep rate and this information allows determining the charge transfer rate constants by applying some model for the theoretical description of the voltammetric response of surface-confined electroactive species.[238–242] However, in the specific case of Pani-like conducting polymers, there are additional features that made the redox switching more complex, such as intrinsic capacitive contributions,[243] ageing effects,[244] coupled proton binding equilibrium,[245,246] effects of mechanical stress,[247,248] potential dependent swelling,[248] hysteresis phenomena,[25] *etc*. In this sense, a quantitative analysis of the voltammetric response of Pani-containing films is difficult mainly due to the lack of a model that accounts for all these features. Nevertheless, the voltammetric response provides valuable information of the redox behavior of Pani-containing films and cyclic voltammetry has become a more direct technique for characterizing the electrochemical performance of Pani-containing LbL-modified electrodes.

A usual problem with Pani-modified electrodes is that Pani is a good electronic conductor and has a stable quasi-reversible electrochemical response in acidic solution but it becomes a poor conductor and is unstable to redox switching. This is a clear disadvantage for its application in bioelectrochemical devices, which operate at near neutral pH. Several strategies have been employed to improve the electronic conductivity and the redox stability of the Pani-based modified-electrodes, such as the incorporation of metal nanoparticles,[249,250] doping with complex anionic molecules[251,252] or polyanions.[253,254]

As the pH increases, the redox potential of the first redox transition of Pani shifts to higher potentials[39,245] whereas the

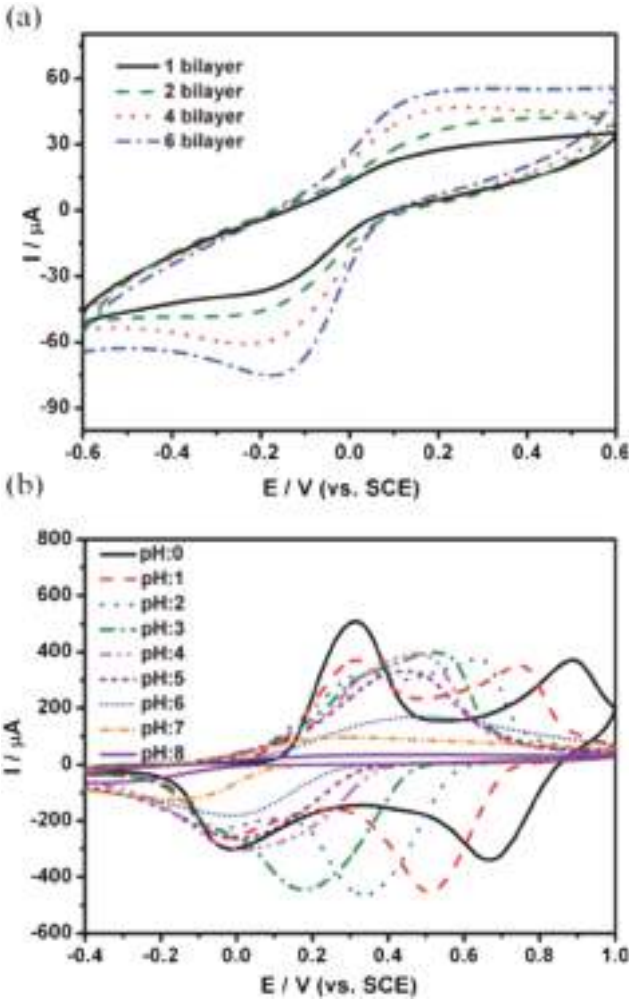

Fig. 15 CV of LbL assembled films of Pani and PSS-capped graphene of different numbers of bilayers in neutral solutions (a) and effect of pH on the voltammetric response (b). Reproduced from ref. 170 with permission from the Royal Society of Chemistry.

second transition shifts to lower potentials. The result is the overlapping of both voltammetric peaks at about neutral pH.[255] The decrease of the electroactivity of Pani at neutral pH is attributedto this overlapping and the low stability to redox switching of the pernigraniline form and its low rate of reduction in these media.

In the particular case of the incorporation of carbon nanomaterials, a clear advantage is the increase of the electronic conductivity which is mainly attributed to the carbonous material and it is not pH dependent. However, when modified materials are employed, the presence of anionic groups can also produce a doping effect by interaction with the charged nitrogen groups of Pani improving both the conductivity of the polymer and the redox response of the whole composite. This is the case of oxidized[125,127] or polymer-capped[124,126] carbon nanotubes as well as oxidized[171] or polymer-capped[170] graphene. The doping effect stabilizes the cyclic voltammetric response at neutral pH, where a single pair of broad peaks indicates the overlapping of the canonical redox transitions of Pani (Fig. 15).[124,126,168,170,171]

The enhanced electroactivity in neutral solution has allowed the development of modified electrodes able to electrochemically interact with bio-relevant species such as NADH,[124] ascorbic acid[171] and H_2O_2 [125,126,170,172] under conditions compatible with biological systems. These materials can also efficiently interact with redox enzymes such as choline oxidase[125] and glucose oxidase[129] providing electronic connections with the electrode without the necessity of redox mediators.

Another common issue in the construction of electroactive films by the LbL method is that sometimes the electrochemical connection between the successive layers and the electrode is not effective and there is a failure of the charge transfer mechanism, which is revealed by a decrease of the voltammetric integrated charge per bilayer as the number of bilayers increases. A usual observed behavior of the voltammetric charge is a linear increment for the first bilayers and then an asymptotic approach to a constant value as the number of bilayers increases. To avoid this problem it is desirable that the counter-part be able to electronically interact with the electrochemically active component providing a good path for the electrons by either electronic conduction or redox mediation without blocking the ionic movements that are needed for charge compensation. Carbon nanomaterials are ideal for this purpose as they have exceptional electronic conductivities and tend to form highly porous structures.[135] For example, in the case of Pani/poly(aminobenzenesulfonic acid)-capped SWNTs, the films show a linear increase of the voltammetric charge on the number of bilayers and the dependence on the sweep rates indicates that there is no diffusional control at least for six

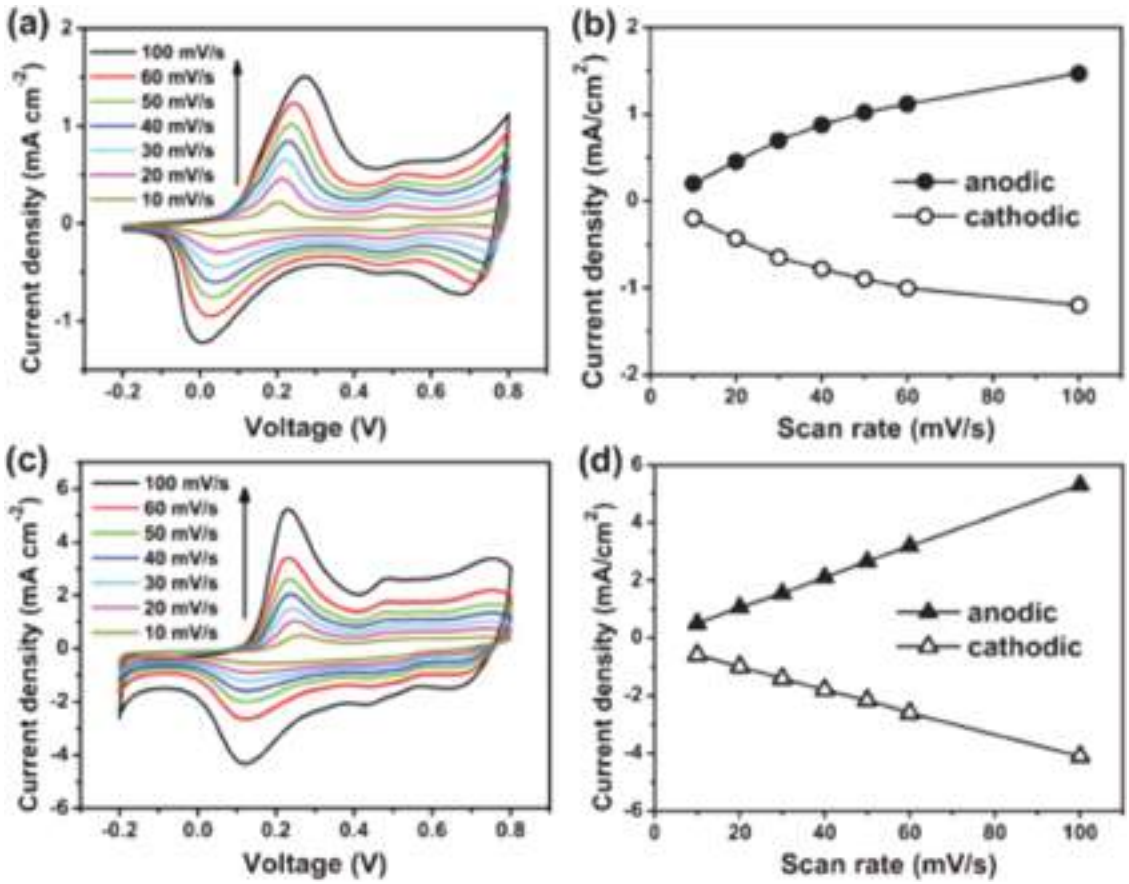

Fig. 16 Effect of sweep rate on the voltammetric response of Pani (a, b) and an LbL of Pani and GO film in acidic solution. Reproduced from ref. 169 with permission from the Royal Society of Chemistry.

bilayers.[124] A similar behavior was observed for 6-bilayers[170] (Fig. 15) and 10-bilayers[171] Pani/rGO films and 8-bilayers Pani/IL-RGO.[172] On the other hand, the voltammetric peak current departs from the linear relation at high sweep rates for 15-bilayer Pani/GO LbL films in neutral solution, which indicates some ionic diffusion limitations (Fig. 16).[167]

The incorporation of carbon nanomaterials also improves the electrochemical response in acidic solution. Compared to a Pani film with the same thickness, a Pani/rGO LbL film showed a more reversible voltammetric response.[169] The peak current increased linearly with the sweep rate for the composite, but it departs from linearity in the case of Pani, showing an ionic transport limitation which in not operative in the first case.

In a recent work, the different dependences of the peak current on the sweep rate for diffusion and non-diffusion-controlled processes have been employed in an approximate method to estimate the proportion of each process in Pani/rGO LbL films in $LiClO_4$ in propylene carbonate. The idea is that diffusion-controlled charge/discharge happens at the outer surface, which is easily accessible. The high proportion of this contribution is attributed to the open porous structure with a high area exposed to the electrolyte (Fig. 17).[183]

3.5.2. Electrochemical capacitors. The electrochemical capacitors (EC), also called supercapacitors or ultracapacitors, are electrochemical devices able to store charge (and energy) by a subnanometric charge separation between the electrolyte and the electrode material.[256] There are two main mechanisms of charge storage. In the electrochemical double-layer capacitors (EDLC) the charge separation is performed within the Helmholtz double-layer set up at the interface of a conducting material immersed in an electrolyte solution. As the energy stored is inversely proportional to the thickness of this double-layer, EDLC have extremely high energy densities. On the other hand, the charge storage can also be achieved by redox reactions, ion intercalation or ionic sorption promoted by polarization of the electrode (a Faradaic process). This phenomenon typically takes place in conducting polymers and metal oxides and it is globally called pseudocapacitance.

The EC performance depends not only on the electrode material and electrolyte but also on the nanoarchitecture of these materials, especially if composites or hybrid materials are employed.[257,258] Fast mechanisms of charge separation and high values of the specific capacitances are desired. This can only be achieved by a precise control of the electrode modification method to obtain relatively high specific areas but maintaining good electronic connectivity within the material.

The excellent mechanical and conduction properties and prominent specific area of carbon nanomaterials made them excellent candidates for the construction of ECs.[259,260] The main charge storage mechanism in carbon based devices is the double-layer capacitance but the specific capacitance can be strongly increased by incorporating other electroactive materials. Conducting polymers can store charge not only by a DL mechanism but also by their rapid reversible electrochemical transformations.[261] In this sense, Pani has been extensively

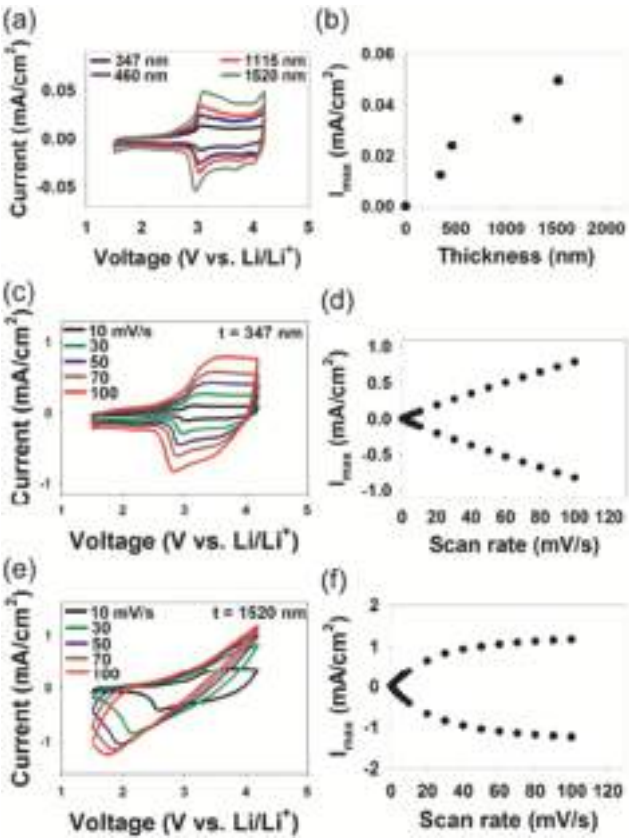

Fig. 17 CV of LbL films of Pani and electrochemically reduced GO of different thicknesses (a, b) and the effect of the sweep rate on the voltammetric response for thin (c, d) and thick (e, f) films. Reproduced from ref. 183 with permission from the Royal Society of Chemistry.

employed as the material for EC owing to low cost, environmental stability, facile synthesis and electrochemical reversibility.[174,175] However, the swelling and shrinkage during the doping/dedoping process and the poor electroactivity in neutral or basic solutions limit its storage capability and cycling performance.

The complementary properties of carbon nanomaterials, mainly graphene, and Pani have recently promoted a great deal of interest in producing composites to be applied in charge storage devices.[262–264] A synergistic effect is attained by the high doping–dedoping rate and the capacity of intercalation between carbon sheets of Pani, and the mechanical stability and good electronic conductivity of graphene (Fig. 18).[33] Several simple synthetic methods have been proposed, but most of them yield hybrid films without a precise control of the architecture (Fig. 19). In contrast, the LbL approach allows obtaining precise control of the film composition, avoiding nanomaterial aggregation by staking and producing an intimate contact between both the components (Fig. 19).[172]

The capacitive performance of film-modified electrodes is mainly evaluated by two types of electrochemical tests. The voltammetric capacitance is evaluated from the integrated electrochemical charge of the voltammogram in a wide potential

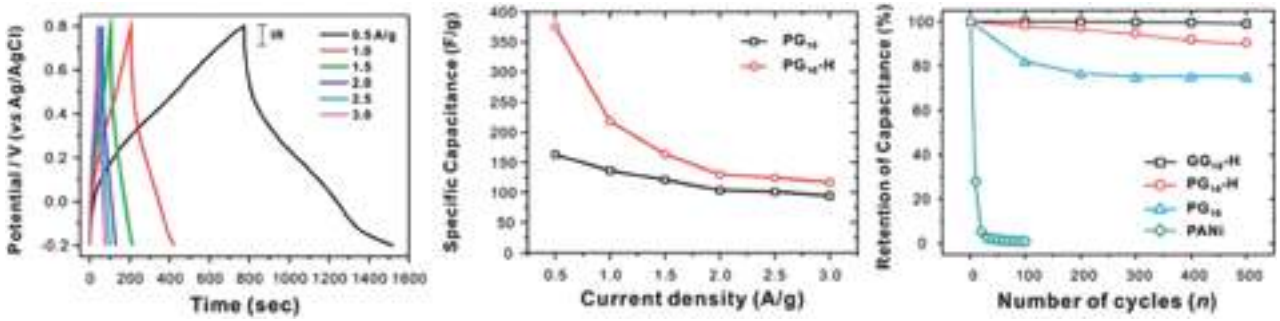

Fig. 18 Galvanostatic charge/discharge curves (left), specific capacitance as a function of the charging current (center) and cycling stability (right) of Pani/GO assemblies in 1 M H_2SO_4. Adapted from ref. 173 with permission from the Royal Society of Chemistry.

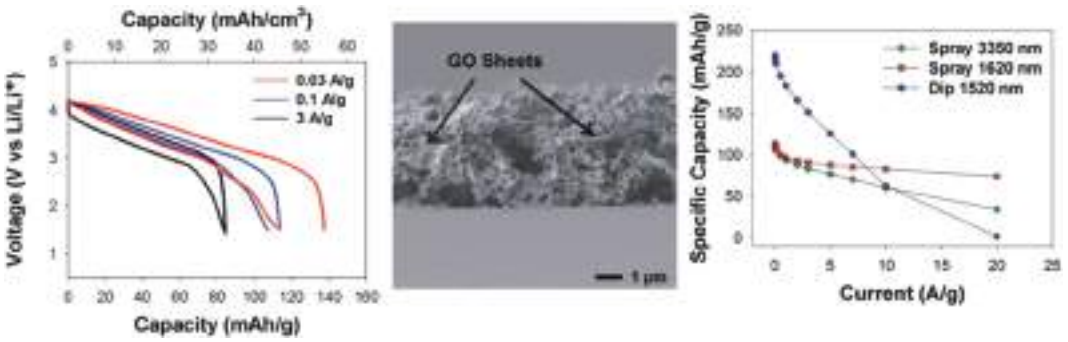

Fig. 19 Voltage *vs.* specific capacity (left) and comparison between specific capacitance of dip-coating and spray-assisted deposited films of Pani nanofibers and electrochemically reduced GO in an organic electrolyte Li cell (right). Cross-sectional SEM image of the spray-assisted assembly (center). Adapted from ref. 184 with permission from the Royal Society of Chemistry.

Table 8 Galvanostatic charge–discharge capacitances for the different Pani/graphene LbL film-modified electrodes

LbL assembly	Conditions	Specific/volumetric/areal capacitance
Pani/rGO[173]	−0.2 to 0.8 V (*vs.* Ag/AgCl) in 1 M H_2SO_4	375–117 F g^{-1} (at 0.5 to 3 A g^{-1})
Pani/rGO[174]	0 to 1 V (*vs.* Ag/AgCl) in 1 M Na_2SO_4	584–170 F cm^{-3} (at 3 to 100 A cm^{-3})
Pani/rGO[175]	−0.2 to 1 (*vs.* Ag/AgCl) in 1 M H_2SO_4	5.16 F cm^{-2} (at 10 mA cm^{-2})
Pani/rGO[206]	−0.2 to 0.8 V (*vs.* Ag/AgCl) in 1 M Na_2SO_4	1563 to 512 F cm^{-3} (at 3 to 100 A cm^{-3})
Pani/GO[177]	−0.2 to 0.8 (*vs.* Ag/AgCl) in 1 M H_2SO_4	1102–733 F cm^{-3} (at 2.5 to 20 A cm^{-3})
Pani/rGO hollow spheres[182]	0 to 0.8 V (*vs.* SCE) in 1 M H_2SO_4	381 F g^{-1} (at 4 A g^{-1})
Pani/rGO[183]	1.5 to 4.2 V (*vs.* Li/Li^+) 0.5 M $LiClO_4$ in propylene carbonate	615–491 F g^{-1} (at 0.1 to 10 A g^{-1})
Pani/rGO[184]	1.5 to 4.2 V (*vs.* Li/Li^+) 0.5 M $LiClO_4$ in propylene carbonate	152–45 F g^{-1} (at 0.03 to 20 A g^{-1})

window, generally recorded at different sweep rates.[173] Another test consists of charging and discharging a cell made by two electrodes by employing a given rate (constant current) between two selected potential limits (Fig. 18). These charge/discharge galvanostatic curves allow the evaluation of the capacitive performance in nearly operative conditions.[173] Additionally, both voltammetric and galvanostatic capacitances usually refer to the amount of electroactive material in mass (specific capacitance) or volume (volumetric capacitance). High areal capacitances are also important for some applications.[185] Although higher areal capacitances are obtained for thicker films, they usually render low volumetric capacitances owing to the difficulty of electronic and ionic conduction across the film.[185]

The galvanostatic capacitances of Pani-containing LbL assemblies evaluated in different solutions are summarized in Table 8.

4. Conclusions and perspectives

The virtues of adopting the layer-by-layer technique as a material processing method are increasingly recognized by the scientific community as well as the technological world. Today, the LbL technique is implicated in a wide range of

applied research fields ranging from biomedical science to photovoltaics. This broadening of the LbL activity also reached the frontiers of carbon nanomaterials and their use in the development of energy storage and sensing applications. Since the start of this decade (the 2010s), carbon nanomaterials research, and especially nanographene research, has blossomed in many different directions, and has attracted a great deal of attention to nanoscience and materials science communities. The variety of examples reviewed here demonstrates that the unique physical, chemical, mechanical, and electronic properties of carbon nanomaterials can be merged with conducting polymers to create nanocomposites exhibiting enhanced electrical conductivities together with physical strength and structural flexibility. However, such a unique combination of characteristics demands the formation of nanoscale uniform blends of nanographene or carbon nanotubes with Pani – a non-trivial task. Additionally, the realization of hybrid interconnected conducting networks usually requires controlled organization of anisotropic nanoscale building blocks such as carbon nanotubes or nanographene sheets, this being considered to be a critical factor for fabricating functional nanocomposites with high nanomaterial contents. Here is where the layer-by-layer assembly comes into the picture as a key enabling methodology facilitating the integration of polymeric and inorganic *partenaires* in a controlled fashion on the electrode support, *i.e.*: nanometer or molecular level control over the integration process.

Seen from an experimental perspective, however, the LbL approach gains even more relevance if we consider that nanostructured films architectured with molecular precision can be readily obtained from the utilization of "wet" chemical and colloid chemical methods. Versatility, flexibility, speed, relative ease of preparation and transfer from the liquid to the solid phase, convenience of scale-up, and economy are the advantages of this chemical approach to produce advanced hybrid interfacial architectures. This has been the key to translate molecular-level systems into the macroscopic world and raise expectations for practical applications. One of the major achievements of this integrative supramolecular concept has been the success in taming structural complexity and functionality as the conducting polymer and the carbon nanomaterials can interact together not only without disrupting their own functions but also producing synergistic effects. As can be concluded from the analysis of the diverse hybrid systems reviewed here, carbon nanomaterials provide a structural framework with excellent electronic connectivity which is essential for the integration of active materials in stable and efficient energy storage devices or the incorporation of transducing elements in a chemical sensor. However, their functions are not merely relegated to structural scaffolds, as they can also act as dopants of the conducting polymer improving its electroactivity, which is important for the construction of biosensors to be employed under physiological conditions. The enhanced electroactivity is also desirable in supercapacitors as it contributes to improve the pseudocapacitance associated with the faradaic process. On the other hand, Pani not only acts as the redox electroactive component but also as a versatile building block for the construction of 3D structures integrating the 1D and 2D-carbon materials.

The examples presented here not only reflect some of the most subtle and delightful facets of the molecular design of supramolecular materials for technological purposes, but also bring into focus many novel aspects of the synthesis, and structural and functional characterization of the obtained hybrid materials. The variety of assemblies of Pani and carbon nanomaterials reviewed here shows that even within the *layer-by-layer paradigm*, a broad spectrum of synthetic routes has been developed pursuing the improvement of some particular desired feature (Scheme 3). In this sense, the LbL construction of conducting polymer/carbon nanomaterial hybrid assemblies could be considered to some extent as an *open-ended story* in which successive efforts will surely lead the subject one step further in the development of more efficient and sensitive electrochemical devices. As such, the purpose of this review has not been solely to provide a broad overview of the LbL construction of Pani and carbon nanomaterials, but to show how integrative supramolecular concepts and "nanoarchitectonics" can be applied to solve emerging technological problems related to energy storage and sensing.

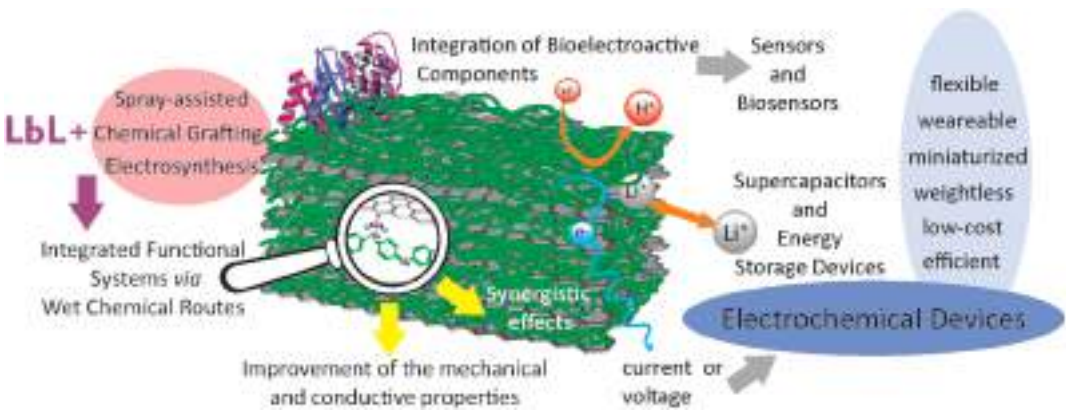

Scheme 3 Perspectives in Pani/carbon nanomaterials LbL assemblies for electrochemical devices.

Acknowledgements

The authors acknowledge financial support from ANPCyT (PICT 2010–2554, PICT-2013-0905), Fundación Petruzza, Universidad Nacional de La Plata (PPID-X009), CONICET (PIP 11220130100370CO), the Marie Curie project "Hierarchical functionalization and assembly of Graphene for multiple device fabrication" (HiGRAPHEN) (Grant ref: 612704), and the Austrian Institute of Technology GmbH (AIT–CONICET Partner Lab: *"Exploratory Research for Advanced Technologies in Supramolecular Materials Science"* – Exp. 4947/11, Res. no. 3911, 28-12-2011). W. A. M. and O. A. are CONICET fellows.

References

1 K. Ariga, M. V. Lee, T. Mori, X.-Y. Yu and J. P. Hill, *Adv. Colloid Interface Sci.*, 2010, **154**, 20–29.
2 M. Aono, Y. Bando and K. Ariga, *Adv. Mater.*, 2012, **24**, 150–151.
3 M. Ramanathan, L. K. Shrestha, T. Mori, Q. Ji, J. P. Hill and K. Ariga, *Phys. Chem. Chem. Phys.*, 2013, **15**, 10580–10611.
4 K. Ariga, Y. Yamauchi, G. Rydzek, Q. Ji, Y. Yonamine, K. C.-W. Wu and J. P. Hill, *Chem. Lett.*, 2014, **43**, 36–68.
5 K. Ariga, Y. Yamauchi and M. Aono, *APL Mater.*, 2015, **3**, 061001.
6 M. Aono and K. Ariga, *Adv. Mater.*, 2016, **28**, 989–992.
7 K. Ariga, Q. Ji, W. Nakanishi, J. P. Hill and M. Aono, *Mater. Horiz.*, 2015, **2**, 406–413.
8 S. K. Vashist, D. Zheng, K. Al-Rubeaan, J. H. T. Luong and F. Sheu, *Biotechnol. Adv.*, 2011, **29**, 169–188.
9 T. Lee, S. H. Min, M. Gu, Y. K. Jung, W. Lee, J. U. Lee, D. G. Seong and B.-S. Kim, *Chem. Mater.*, 2015, **27**, 3785–3796.
10 C. Soldano, A. Mahmood and E. Dujardin, *Carbon*, 2010, **48**, 2127–2150.
11 G. Nyström, A. Marais, E. Karabulut, L. Wågberg, Y. Cui and M. M. Hamedi, *Nat. Commun.*, 2015, **6**, 7259.
12 L. Wang, X. Lu, S. Lei and Y. Song, *J. Mater. Chem. A*, 2014, **2**, 4491–4509.
13 M. M. Islam, S. H. Aboutalebi, D. Cardillo, H. K. Liu, K. Konstantinov and S. X. Dou, *ACS Cent. Sci.*, 2015, **1**, 206–216.
14 N. Ashok Kumar and J. Baek, *Chem. Commun.*, 2014, **50**, 6298–6308.
15 G. Decher and J.-D. Hong, *Makromol. Chem., Macromol. Symp.*, 1991, **46**, 321–327.
16 G. Decher, B. Lehr, K. Lowack, Y. Lvov and J. Schmitt, *Biosens. Bioelectron.*, 1994, **9**, 677–684.
17 G. Decher, J. D. Hong and J. Schmitt, *Thin Solid Films*, 1992, **210–211**, 831–835.
18 G. Decher, Y. Lvov and J. Schmitt, *Thin Solid Films*, 1994, **244**, 772–777.
19 Y. T. Park and J. C. Grunlan, in *Multilayer Thin Films*, Wiley-VCH Verlag GmbH & Co. KGaA, Weinheim, Germany, 2012, vol. 2, pp. 595–612.
20 P. T. Hammond, *Adv. Mater.*, 2004, **16**, 1271–1293.
21 G. Rydzek, Q. Ji, M. Li, P. Schaaf, J. P. Hill, F. Boulmedais and K. Ariga, *Nano Today*, 2015, **10**, 138–167.
22 P. T. Hammond, *AIChE J.*, 2011, **57**, 2928–2940.
23 J. L. Lutkenhaus and P. T. Hammond, *Soft Matter*, 2007, **3**, 804–816.
24 G. Inzelt, *J. Solid State Electrochem.*, 2011, **15**, 1711–1718.
25 G. Inzelt, *Conducting Polymers: A New Era in Electrochemsitry*, Springer-Verlag, Berlin Heidelberg, 2nd edn, 2012.
26 J. Heinze, B. A. Frontana-Uribe and S. Ludwigs, *Chem. Rev.*, 2010, **110**, 4724–4771.
27 S. Bhadra, D. Khastgir, N. K. Singha and J. H. Lee, *Prog. Polym. Sci.*, 2009, **34**, 783–810.
28 G. Ćirić-Marjanović, *Synth. Met.*, 2013, **177**, 1–47.
29 J. Stejskal, M. Trchová, P. Bober, P. Humpolíček, V. Kašpárková, I. Sapurina, M. A. Shishov and M. Varga, in *Encyclopedia of Polymer Science and Technology*, John Wiley & Sons, Inc., 2015.
30 J. Xie, X. Han, C. Zong, H. Ji and C. Lu, *Macromolecules*, 2015, **48**, 663–671.
31 C. Dhand, M. Das, M. Datta and B. D. Malhotra, *Biosens. Bioelectron.*, 2011, **26**, 2811–2821.
32 M. Jaymand, *Prog. Polym. Sci.*, 2013, **38**, 1287–1306.
33 N. A. Kumar and J.-B. Baek, *Chem. Commun.*, 2014, **50**, 6298–6308.
34 C. Desmet, C. A. Marquette, L. J. Blum and B. Doumèche, *Biosens. Bioelectron.*, 2016, **76**, 145–163.
35 N. J. Ronkainen, H. B. Halsall and W. R. Heineman, *Chem. Soc. Rev.*, 2010, **39**, 1747–1763.
36 R. M. Iost and F. N. Crespilho, *Biosens. Bioelectron.*, 2012, **31**, 1–10.
37 E. Kang, K. G. Neoh and K. L. Tan, *Prog. Polym. Sci.*, 1998, **23**, 277–324.
38 J. E. Albuquerque, L. H. C. Mattoso, D. T. Balogh, R. M. Faria, J. G. Masters and A. G. MacDiarmid, *Synth. Met.*, 2000, **113**, 19–22.
39 W. A. Marmisollé, M. I. Florit and D. Posadas, *J. Electroanal. Chem.*, 2014, **734**, 10–17.
40 A. G. MacDiarmid and A. J. Epstein, *Faraday Discuss. Chem. Soc.*, 1989, **88**, 317–322.
41 W. S. Huang and A. G. MacDiarmid, *Polymer*, 1993, **34**, 1833–1845.
42 A. Petr, A. Neudeck and L. Dunsch, *Chem. Phys. Lett.*, 2005, **401**, 130–134.
43 L. Lizarraga, E. M. Andrade, M. I. Florit and F. V. Molina, *J. Phys. Chem. B*, 2005, **109**, 18815–18821.
44 S. Stafström, J. L. Brédas, A. J. Epstein, H. S. Woo, D. B. Tanner, W. S. Huang and A. G. MacDiarmid, *Phys. Rev. Lett.*, 1987, **59**, 1464–1467.
45 J. L. Delgado, M. Herranz and N. Martín, *J. Mater. Chem.*, 2008, **18**, 1417–1426.
46 D. Jariwala, V. K. Sangwan, L. J. Lauhon, T. J. Marks and M. C. Hersam, *Chem. Soc. Rev.*, 2013, **42**, 2824–2860.

47 Q. Zhang, J. Q. Huang, W. Z. Qian, Y. Y. Zhang and F. Wei, *Small*, 2013, **9**, 1237–1265.
48 L. Dai, D. W. Chang, J.-B. Baek and W. Lu, *Small*, 2012, **8**, 1130–1166.
49 H. Wang, Q. Hao, X. Yang, L. Lu and X. Wang, *Electrochem. Commun.*, 2009, **11**, 1158–1161.
50 Y. Zhu, S. Murali, M. D. Stoller, K. J. Ganesh, W. Cai, P. J. Ferreira, A. Pirkle, R. M. Wallace, K. a. Cychosz, M. Thommes, D. Su, E. a. Stach and R. S. Ruoff, *Science*, 2011, **332**, 1537–1541.
51 M. M. Barsan, M. E. Ghica and C. M. A. Brett, *Anal. Chim. Acta*, 2015, **881**, 1–23.
52 M. S. Dresselhaus, G. Dresselhaus and A. Jorio, *Annu. Rev. Mater. Res.*, 2004, **34**, 247–278.
53 E. T. Thostenson, Z. Ren and T.-W. Chou, *Compos. Sci. Technol.*, 2001, **61**, 1899–1912.
54 E. Fitzer, K.-H. Kochling, H. P. Boehm and H. Marsh, *Pure Appl. Chem.*, 1995, **67**, 473–506.
55 A. Ambrosi, C. K. Chua, A. Bonanni and M. Pumera, *Chem. Rev.*, 2014, **114**, 7150–7188.
56 O. C. Compton and S. T. Nguyen, *Small*, 2010, **6**, 711–723.
57 G. Eda and M. Chhowalla, *Adv. Mater.*, 2010, **22**, 2392–2415.
58 D. C. Marcano, D. V. Kosynkin, J. M. Berlin, A. Sinitskii, Z. Sun, A. Slesarev, L. B. Alemany, W. Lu and J. M. Tour, *ACS Nano*, 2010, **4**, 4806–4814.
59 W. S. Hummers and R. E. Offeman, *J. Am. Chem. Soc.*, 1958, **80**, 1339–1339.
60 A. C. Fou and M. F. Rubner, *Macromolecules*, 1995, **28**, 7115–7120.
61 J. H. Cheung, W. B. Stockton and M. F. Rubner, *Macromolecules*, 1997, **30**, 2712–2716.
62 W. B. Stockton and M. F. Rubner, *Macromolecules*, 1997, **30**, 2717–2725.
63 D. Li, Y. Jiang, Z. Wu, X. Chen and Y. Li, *Thin Solid Films*, 2000, **360**, 24–27.
64 M. K. Ram, M. Salerno, M. Adami, P. Faraci and C. Nicolini, *Langmuir*, 1999, **13**, 1252–1259.
65 G. S. Braga, L. G. Paterno, J. P. H. Lima, F. J. Fonseca and A. M. de Andrade, *Mater. Sci. Eng., C*, 2008, **28**, 555–562.
66 F. R. Simoes, L. a. Pocrifka, L. F. Q. P. Marchesi and E. C. Pereira, *J. Phys. Chem. B*, 2011, **115**, 11092–11097.
67 M.-K. Park, K. Onishi, J. Locklin, F. Caruso and R. C. Advincula, *Langmuir*, 2003, **19**, 8550–8554.
68 J. He, R. Li and F. Gu, *J. Appl. Polym. Sci.*, 2013, **128**, 1673–1679.
69 D. J. Schmidt, E. M. Pridgen, P. T. Hammond and J. Christopher Love, *J. Chem. Educ.*, 2010, **87**, 208–211.
70 D. Li, Y. Jiang, C. Li, Z. Wu, X. Chen and Y. Li, *Polymer*, 1999, **40**, 7065–7070.
71 C. Ge, W. J. Doherty, S. B. Mendes, N. R. Armstrong and S. S. Saavedra, *Talanta*, 2005, **65**, 1126–1131.
72 C. Ge, N. R. Armstrong and S. S. Saavedra, *Anal. Chem.*, 2007, **79**, 1401–1410.
73 Z. Hu, J. Xu, Y. Tian, R. Peng, Y. Xian, Q. Ran and L. Jin, *Electrochim. Acta*, 2009, **54**, 4056–4061.
74 H. Barrientos, I. Moggio, E. Arias-Marin, A. Ledezma and J. Romero, *Eur. Polym. J.*, 2007, **43**, 1672–1680.
75 H. Zhang, X. Yan, Y. Wang, Y. Deng and X. Wang, *Polymer*, 2008, **49**, 5504–5512.
76 M. C. Santos, M. L. Munford and R. F. Bianchi, *Mater. Sci. Eng., B*, 2012, **177**, 359–366.
77 J. Travas-Sejdic, R. Soman and H. Peng, *Thin Solid Films*, 2006, **497**, 96–102.
78 L. F. Marchesi, S. C. Jacumasso, R. C. Quintanilha, H. Winnischofer and M. Vidotti, *Electrochim. Acta*, 2015, **174**, 864–870.
79 C. Li, K. Mitamura and T. Imae, *Macromol. Rapid Commun.*, 2003, **36**, 9957–9965.
80 R. Nohria, R. K. Khillan, Y. Su, R. Dikshit, Y. Lvov and K. Varahramyan, *Sens. Actuators, B*, 2006, **114**, 218–222.
81 J. Grochol, R. Dronov, F. Lisdat, P. Hildebrandt and D. H. Murgida, *Langmuir*, 2007, **23**, 11289–11294.
82 C. Kepplinger, F. Lisdat and U. Wollenberger, *Langmuir*, 2011, **27**, 8309–8315.
83 R. Spricigo, R. Dronov, K. V. Rajagopalan, F. Lisdat, S. Leimkühler, F. W. Scheller and U. Wollenberger, *Soft Matter*, 2008, **4**, 972–978.
84 R. Dronov, D. G. Kurth, H. Möhwald, F. W. Scheller and F. Lisdat, *Electrochim. Acta*, 2007, **53**, 1107–1113.
85 F. Wegerich, P. Turano, M. Allegrozzi, H. Möhwald and F. Lisdat, *Langmuir*, 2011, **27**, 4202–4211.
86 R. Dronov, D. G. Kurth, H. Möhwald, F. W. Scheller and F. Lisdat, *Angew. Chem., Int. Ed.*, 2008, **47**, 3000–3003.
87 S. Jung, H. Kim, M. Han, Y. Kang and E. Kim, *Mater. Sci. Eng., C*, 2004, **24**, 57–60.
88 D. DeLongchamp and P. T. Hammond, *Adv. Mater.*, 2001, **13**, 1455–1459.
89 T. R. Farhat and P. T. Hammond, *Chem. Mater.*, 2006, **18**, 41–49.
90 A. Baba, M. K. Park, R. C. Advincula and W. Knoll, *Langmuir*, 2002, **18**, 4648–4652.
91 R. Montazami, V. Jain and J. R. Heflin, *Electrochim. Acta*, 2010, **56**, 990–994.
92 N. Zhang, R. Schweiss and W. Knoll, *J. Solid State Electrochem.*, 2007, **11**, 451–456.
93 S. Tian, A. Baba, J. Liu, Z. Wang, W. Knoll, M. K. Park and R. Advincula, *Adv. Funct. Mater.*, 2003, **13**, 473–479.
94 J. W. Jeon, J. O'Neal, L. Shao and J. L. Lutkenhaus, *ACS Appl. Mater. Interfaces*, 2013, **5**, 10127–10136.
95 U. Lange, S. Ivanov, V. Lyutov, V. Tsakova and V. M. Mirsky, *J. Solid State Electrochem.*, 2010, **14**, 1261–1268.
96 A. Stoyanova, S. Ivanov, V. Tsakova and A. Bund, *Electrochim. Acta*, 2011, **56**, 3693–3699.
97 S. Tian, J. Liu, T. Zhu and W. Knoll, *Chem. Mater.*, 2004, **16**, 4103–4108.
98 H. Lin, J. Yang, J. Liu, Y. Huang, J. Xiao and X. Zhang, *Electrochim. Acta*, 2013, **90**, 382–392.
99 S. Ivanov, U. Lange, V. Tsakova and V. M. Mirsky, *Sens. Actuators, B*, 2010, **150**, 271–278.

100 F. Huguenin, M. Ferreira, V. Zucolotto, F. C. Nart, R. M. Torresi and O. N. Oliveira, *Chem. Mater.*, 2004, **16**, 2293–2299.

101 R. Schweiss, N. Zhang and W. Knoll, *J. Sol–Gel Sci. Technol.*, 2007, **44**, 1–5.

102 F. Huguenin, F. C. Nart, E. R. Gonzalez and O. N. Oliveira, *J. Phys. Chem. B*, 2004, **108**, 18919–18924.

103 L. Shao, J.-W. Jeon and J. L. Lutkenhaus, *J. Mater. Chem. A*, 2013, **1**, 7648–7656.

104 M. Ferreira, F. Huguenin, V. Zucolotto, E. Pereira, S. I. Co, D. Torresi, L. a. Temperini and R. M. Torresi, *J. Phys. Chem.*, 2003, **107**, 8351–8354.

105 L. Shao, J.-W. Jeon and J. L. Lutkenhaus, *J. Mater. Chem. A*, 2014, **2**, 14421–14428.

106 D. M. DeLongchamp and P. T. Hammond, *Chem. Mater.*, 2004, **16**, 4799–4805.

107 D. Li, Y. Jiang, Z. Wu, X. Chen and Y. Li, *Sens. Actuators, B*, 2000, **66**, 125–127.

108 Y. Wang, C. Guo, Y. Chen, C. Hu and W. Yu, *J. Colloid Interface Sci.*, 2003, **264**, 176–183.

109 C. Zhao, H. Lin, Q. Zhang and H. Na, *Int. J. Hydrogen Energy*, 2010, **35**, 10482–10488.

110 C. H. B. Silva, N. A. Galiote, F. Huguenin, É. Teixeira-Neto, V. R. L. Constantino and M. L. A. Temperini, *J. Mater. Chem.*, 2012, **22**, 14052–14060.

111 S. Yu, M. Xi, K. Han, Z. Wang, W. Yang and H. Zhu, *Thin Solid Films*, 2010, **519**, 357–361.

112 A. de Barros, M. Ferreira, C. J. L. Constantino and M. Ferreira, *Synth. Met.*, 2014, **197**, 119–125.

113 W. Feng, F. Zhou, X. Wang, X. Bai, J. Liang and K. Yoshino, *Jpn. J. Appl. Phys.*, 2003, **42**, 5726–5730.

114 N. I. Kovtyukhova and T. E. Mallouk, *J. Phys. Chem. B*, 2005, **109**, 2540–2545.

115 X. Yan, Z. Han, Y. Yang and B. Tay, *J. Phys. Chem. C*, 2007, **111**, 4125–4131.

116 F. Wang, G. Wang, S. Yang and C. Li, *Langmuir*, 2008, **24**, 5825–5831.

117 E. Detsri and S. T. Dubas, *Colloids Surf., A*, 2014, **444**, 89–94.

118 M. Kaempgen and S. Roth, *J. Electroanal. Chem.*, 2006, **586**, 72–76.

119 K. J. Loh, J. Kim, J. P. Lynch, N. W. S. Kam and N. A. Kotov, *Smart Mater. Struct.*, 2007, **16**, 429–438.

120 T.-C. Hou, K. J. Loh and J. P. Lynch, *Nanotechnology*, 2007, **18**, 315501.

121 K. J. Loh, J. P. Lynch and N. A. Kotov, *Smart Struct. Syst.*, 2008, **4**, 531–548.

122 A. Vandenberg and K. J. Loh, *Nano Life*, 2012, **2**, 1242001.

123 J. Lu, B. J. Park, B. Kumar, M. Castro, H. J. Choi and J.-F. Feller, *Nanotechnology*, 2010, **21**, 255501.

124 J. Liu, S. Tian and W. Knoll, *Langmuir*, 2005, **21**, 5596–5599.

125 F. Qu, M. Yang, J. Jiang, G. Shen and R. Yu, *Anal. Biochem.*, 2005, **344**, 108–114.

126 Z. Hu, J. Xu, Y. Tian, R. Peng, Y. Xian, Q. Ran and L. Jin, *Carbon*, 2010, **48**, 3729–3736.

127 J. S. Silva, A. de Barros, C. J. L. Constantino, F. R. Simoes and M. Ferreira, *J. Nanosci. Nanotechnol.*, 2014, **14**, 6586–6592.

128 T. Rosa, G. J. R. Aroeira, L. S. Parreira, L. Codognoto, M. C. Santos and F. R. Simões, *Synth. Met.*, 2015, **210**, 186–191.

129 S. Komathi, A. I. Gopalan and K. P. Lee, *Biosens. Bioelectron.*, 2009, **24**, 3131–3134.

130 A. D. Taylor, M. Michel, R. C. Sekol, J. M. Kizuka, N. A. Kotov and L. T. Thompson, *Adv. Funct. Mater.*, 2008, **18**, 3003–3009.

131 A. Wolz, S. Zils, M. Michel and C. Roth, *J. Power Sources*, 2010, **195**, 8162–8167.

132 E. N. Konyushenko, J. Stejskal, M. Trchová, J. Hradil, J. Kovářová, J. Prokeš, M. Cieslar, J. Y. Hwang, K. H. Chen and I. Sapurina, *Polymer*, 2006, **47**, 5715–5723.

133 I. Sapurina and J. Stejskal, *Chem. Pap.*, 2009, **63**, 579–585.

134 L. Q. Hoa, Y. Sugano, H. Yoshikawa, M. Saito and E. Tamiya, *Electrochim. Acta*, 2011, **56**, 9875–9882.

135 N. Hyder, S. W. Lee, F. C. Cebeci, D. J. Schmidt, Y. Shao-Horn and P. T. Hammond, *ACS Nano*, 2011, **5**, 8552–8561.

136 N. A. Kotov, I. Dékány and J. H. Fendler, *Adv. Mater.*, 1996, **8**, 637–641.

137 T. Cassagneau, F. Gurin and J. H. Fendler, *Langmuir*, 2000, 7318–7324.

138 T. Cassagneau and J. Fendler, *Adv. Mater.*, 1998, **10**, 877–881.

139 T. Cassagneau and J. H. Fendler, *J. Phys. Chem. B*, 1999, **103**, 1789–1793.

140 N. I. Kovtyukhova, P. J. Ollivier, B. R. Martin, T. E. Mallouk, S. A. Chizhik, E. V. Buzaneva and A. D. Gorchinskiy, *Chem. Mater.*, 1999, **11**, 771–778.

141 T. Szabó, A. Szeri and I. Dékány, *Carbon*, 2005, **43**, 87–94.

142 P. G. Su and K. H. Cheng, *Sens. Actuators, B*, 2009, **142**, 123–129.

143 Z. Lei, T. Mitsui, H. Nakafuji, M. Itagaki and W. Sugimoto, *J. Phys. Chem. C*, 2014, **118**, 6624–6630.

144 S. Liu, J. Ou, Z. Li, S. Yang and J. Wang, *Appl. Surf. Sci.*, 2012, **258**, 2231–2236.

145 M. Hu and B. Mi, *J. Membr. Sci.*, 2014, **469**, 80–87.

146 J. Wu, Q. Tang, H. Sun, J. Lin, H. Ao, M. Huang and Y. Huang, *Langmuir*, 2008, **24**, 4801–4805.

147 Q. Tang, J. Wu, Q. Li and J. Lin, *Polymer*, 2008, **49**, 5329–5335.

148 J. Shen, Y. Hu, C. Li, C. Qin, M. Shi and M. Ye, *Langmuir*, 2009, **25**, 6122–6128.

149 A. Rani, K. A. Oh, H. Koo, H. J. Lee and M. Park, *Appl. Surf. Sci.*, 2011, **257**, 4982–4989.

150 J. Zhu and J. He, *Nanoscale*, 2012, **4**, 3558.

151 B.-S. Kong, J. Geng and H.-T. Jung, *Chem. Commun.*, 2009, 2174–2176.

152 D. Chen, X. Wang, T. Liu, X. Wang and J. Li, *ACS Appl. Mater. Interfaces*, 2010, **2**, 2005–2011.

153 H.-B. Yao, L.-H. Wu, C.-H. Cui, H.-Y. Fang and S.-H. Yu, *J. Mater. Chem.*, 2010, **20**, 5190–5195.

154 Q. Ji, I. Honma, S. M. Paek, M. Akada, J. P. Hill, A. Vinu and K. Ariga, *Angew. Chem., Int. Ed.*, 2010, **49**, 9737–9739.

155 C. Zhu, S. Guo, Y. Zhai and S. Dong, *Langmuir*, 2010, **26**, 7614–7618.
156 D. W. Lee, T.-K. Hong, D. Kang, J. Lee, M. Heo, J. Y. Kim, B.-S. Kim and H. S. Shin, *J. Mater. Chem.*, 2011, **21**, 3438–3442.
157 J. S. Park, S. M. Cho, W.-J. Kim, J. Park and P. J. Yoo, *ACS Appl. Mater. Interfaces*, 2011, **3**, 360–368.
158 H. Hwang, P. Joo, M. S. Kang, G. Ahn, J. T. Han, B. S. Kim and J. H. Cho, *ACS Nano*, 2012, **6**, 2432–2440.
159 D. Wang and X. Wang, *Langmuir*, 2011, **27**, 2007–2013.
160 H. Li, S. Pang, S. Wu, X. Feng, K. Müllen and C. Bubeck, *J. Am. Chem. Soc.*, 2011, **133**, 9423–9429.
161 A. Yu, H. W. Park, A. Davies, D. C. Higgins, Z. Chen and X. Xiao, *J. Phys. Chem. Lett.*, 2011, **2**, 1855–1860.
162 X. Liu, H. Zhu and X. Yang, *Talanta*, 2011, **87**, 243–248.
163 W. H. Khoh and J. D. Hong, *Colloids Surf., A*, 2013, **436**, 104–112.
164 Y. Zhou, J. Yang, X. Cheng, N. Zhao, L. Sun, H. Sun and D. Li, *Carbon*, 2012, **50**, 4343–4350.
165 Z. S. Wu, K. Parvez, A. Winter, H. Vieker, X. Liu, S. Han, A. Turchanin, X. Feng and K. Müllen, *Adv. Mater.*, 2014, **26**, 4552–4558.
166 W. Yang, Z.-B. Zheng, T.-T. Meng and K.-Z. Wang, *J. Mater. Chem. A*, 2015, **3**, 3441–3449.
167 K. Sheng, H. Bai, Y. Sun, C. Li and G. Shi, *Polymer*, 2011, **52**, 5567–5572.
168 Y. Tang, N. Wu, S. Luo, C. Liu, K. Wang and L. Chen, *Macromol. Rapid Commun.*, 2012, **33**, 1780–1786.
169 J. Lu, W. Liu, H. Ling, J. Kong, G. Ding, D. Zhou and X. Lu, *RSC Adv.*, 2012, **2**, 10537–10543.
170 J. Luo, Y. Chen, Q. Ma, R. Liu and X. Liu, *RSC Adv.*, 2013, **3**, 17866–17673.
171 J. Cong, Y. Chen, J. Luo and X. Liu, *J. Solid State Chem.*, 2014, **218**, 171–177.
172 J. Luo, R. Liu and X. Liu, *J. Mater. Chem. C*, 2014, **2**, 4818–4827.
173 T. Lee, T. Yun, B. Park, B. Sharma, H.-K. Song and B.-S. Kim, *J. Mater. Chem.*, 2012, **22**, 21092–21099.
174 A. K. Sarker and J.-D. Hong, *Langmuir*, 2012, **28**, 12637–12646.
175 Z. Gao, W. Yang, J. Wang, H. Yan, Y. Yao, J. Ma, B. Wang, M. Zhang and L. Liu, *Electrochim. Acta*, 2013, **91**, 185–194.
176 E. Mitchell, J. Candler, F. De Souza, R. K. Gupta, B. K. Gupta and L. F. Dong, *Synth. Met.*, 2015, **199**, 214–218.
177 B. Wee and J. Hong, *Langmuir*, 2014, **30**, 5267–5275.
178 H. Cai, Q. Tang, B. He, M. Wang, S. Yuan and H. Chen, *Electrochim. Acta*, 2014, **121**, 136–142.
179 K. Saranya, M. Rameez and A. Subramania, *Eur. Polym. J.*, 2015, **66**, 207–227.
180 M. Wang, Q. Tang, H. Chen and B. He, *Electrochim. Acta*, 2014, **125**, 510–515.
181 P. Yang, J. Duan, D. Liu, Q. Tang and B. He, *Electrochim. Acta*, 2015, **173**, 331–337.
182 J. Luo, Q. Ma, H. Gu, Y. Zheng and X. Liu, *Electrochim. Acta*, 2015, **173**, 184–192.
183 J.-W. Jeon, S. R. Kwon and J. L. Lutkenhaus, *J. Mater. Chem. A*, 2015, **3**, 3757–3767.
184 S. R. Kwon, J.-W. Jeon and J. L. Lutkenhaus, *RSC Adv.*, 2015, **5**, 14994–15001.
185 Z.-S. Wu, K. Parvez, S. Li, S. Yang, Z. Liu, S. Liu, X. Feng and K. Müllen, *Adv. Mater.*, 2015, **27**, 4054–4061.
186 Y. H. Kim, C. Foster, J. Chiang and A. J. Heeger, *Synth. Met.*, 1988, **26**, 49–59.
187 D. E. Stilwell and S. Park, *J. Electroanal. Chem.*, 1989, **136**, 427–433.
188 J. Ginder and A. Epstein, *Phys. Rev. B: Condens. Matter*, 1990, **41**, 10674–10685.
189 J. G. Masters, J. M. Ginder, A. G. Macdiarmid and A. J. Epstein, *J. Chem. Phys.*, 1992, **96**, 4768–4778.
190 R. P. McCall, J. M. Ginder, J. M. Leng, H. J. Ye, S. K. Manohar, J. G. Masters, G. E. Asturias, A. G. MacDiarmid and A. J. Epstein, *Phys. Rev. B: Condens. Matter*, 1990, **41**, 5202–5213.
191 D. Chinn, J. DuBow, J. Li, J. Janata and M. Josowicz, *Chem. Mater.*, 1995, **7**, 1510–1518.
192 D. Kumar, *Eur. Polym. J.*, 1999, **35**, 1919–1923.
193 S. Stafström and J. L. Brédas, *Mol. Cryst. Liq. Cryst. Inc. Nonlinear Opt.*, 1988, **160**, 405–420.
194 J. Yue, Z. Wang, K. R. Cromack, A. J. Epstein and A. G. Macdiarmid, *J. Am. Chem. Soc.*, 1991, **113**, 2665–2671.
195 N. S. Sariciftci, L. Smilowitz, Y. Cao and A. J. Heeger, *J. Chem. Phys.*, 1993, **98**, 2664–2669.
196 Z. T. de Oliveira Jr. and M. C. dos Santos, *Chem. Phys.*, 2000, **260**, 95–103.
197 V. N. Popov, *Mater. Sci. Eng., R*, 2004, **43**, 61–102.
198 T. Ohta, A. Bostwick, T. Seyller, K. Horn and E. Rotenberg, *Science*, 2006, **313**, 951–954.
199 Z. Luo, P. M. Vora, E. J. Mele, A. T. C. Johnson and J. M. Kikkawa, *Appl. Phys. Lett.*, 2009, **94**, 111909.
200 K. P. Loh, Q. Bao, G. Eda and M. Chhowalla, *Nat. Chem.*, 2010, **2**, 1015–1024.
201 I. K. Moon, J. Lee, R. S. Ruoff and H. Lee, *Nat. Commun.*, 2010, **1**, 1–6.
202 R. Sainz, A. M. Benito, M. T. Martínez, J. F. Galindo, J. Sotres, A. M. Baró, B. Corraze, O. Chauvet and W. K. Maser, *Adv. Mater.*, 2005, **17**, 278–281.
203 M. in het Panhuis, R. Sainz, P. C. Innis, L. a. P. Kane-Maguire, A. M. Benito, M. T. Martínez, S. E. Moulton, G. G. Wallace and W. K. Maser, *J. Phys. Chem. B*, 2005, **109**, 22725–22729.
204 C. Dhand, S. K. Arya, S. P. Singh, B. P. Singh, M. Datta and B. D. Malhotra, *Carbon*, 2008, **46**, 1727–1735.
205 J. Zhang, H. Yang, G. Shen, P. Cheng, J. Zhang and S. Guo, *Chem. Commun.*, 2010, **46**, 1112–1114.
206 A. K. Sarker and J.-D. Hong, *Colloids Surf., A*, 2013, **436**, 967–974.
207 F. Smits, *Bell Syst. Tech. J.*, 1958, 711–718.
208 A. C. C. Ferrari and D. M. M. Basko, *Nat. Nanotechnol.*, 2013, **8**, 235–246.
209 M. S. Dresselhaus, G. Dresselhaus, R. Saito and A. Jorio, *Phys. Rep.*, 2005, **409**, 47–99.

210 M. Kalbac, J. Kong and M. S. Dresselhaus, *J. Phys. Chem. C*, 2012, **116**, 19046–19050.
211 Z. H. Ni, T. Yu, Y. H. Lu, Y. Y. Wang, Y. P. Feng and Z. X. Shen, *ACS Nano*, 2008, **2**, 2301–2305.
212 S. Nanot, M. Millot, B. Raquet, J.-M. Broto, A. Magrez and J. Gonzalez, *Phys. E*, 2010, **42**, 2466–2470.
213 I. Calizo, A. A. Balandin, W. Bao, F. Miao and C. N. Lau, *Nano Lett.*, 2007, **7**, 2645–2649.
214 Y. Furukawa, F. Ueda, Y. Hyodo, I. Harada, T. Nakajima and T. Kawagoe, *Macromolecules*, 1988, **21**, 1297–1305.
215 M. Bartonek, N. S. Sariciftci and H. Kuzmany, *Synth. Met.*, 1990, **36**, 83–93.
216 M. Ohira, T. Sakai, M. Takeuchi, Y. Kobayashi and M. Tsuji, *Synth. Met.*, 1987, **18**, 347–352.
217 J. Laska, *Synth. Met.*, 2002, **129**, 229–233.
218 S. Quillard, K. Berrada, G. Louam and S. Lefrant, *Synth. Met.*, 1995, **69**, 201–204.
219 R. Mazeikiene, A. Statino, Z. Kuodis, G. Niaura and A. Malinauskas, *Electrochem. Commun.*, 2006, **8**, 1082–1086.
220 X. Yan, Z. Han, Y. Yang and B. Tay, *J. Phys. Chem. C*, 2007, **3**, 4125–4131.
221 S. Chen and H. Lee, *Macromol. Biosci.*, 1993, **26**, 3254–3261.
222 H. K. Chaudhari and D. S. Kelkar, *J. Appl. Polym. Sci.*, 1996, **62**, 15–18.
223 P.-Y. Chen, N.-M. N.-M. Dorval Courchesne, M. N. Hyder, J. Qi, A. M. Belcher and P. T. Hammond, *RSC Adv.*, 2015, **5**, 37970–37977.
224 L. Zhang, J. Liang, Y. Huang, Y. Ma, Y. Wang and Y. Chen, *Carbon*, 2009, **47**, 3365–3368.
225 W. A. Marmisollé, D. Gregurec, S. Moya and O. Azzaroni, *ChemElectroChem*, 2015, **2**, 2011–2019.
226 J. Yue and A. Epstein, *Macromolecules*, 1991, **24**, 4441–4445.
227 S. Kumar, F. Gaillard, G. Bouyssoux and A. Sartre, *Synth. Met.*, 1990, **36**, 111–127.
228 C. Hennig, K. H. Hallmeier and R. Szargan, *Synth. Met.*, 1998, **92**, 161–166.
229 S. Golczak, A. Kanciurzewska, M. Fahlman, K. Langer and J. Langer, *Solid State Ionics*, 2008, **179**, 2234–2239.
230 E. Kang, K. Neoh and K. Tan, *Polymer*, 1994, **35**, 3193–3199.
231 H. Ago, T. Kugler, F. Cacialli, W. R. Salaneck, M. S. P. Shaffer, A. H. Windle and R. H. Friend, *J. Phys. Chem. B*, 1999, **103**, 8116–8121.
232 V. Datsyuk, M. Kalyva, K. Papagelis, J. Parthenios, D. Tasis, A. Siokou, I. Kallitsis and C. Galiotis, *Carbon*, 2008, **46**, 833–840.
233 S. Kundu, Y. Wang, W. Xia and M. Muhler, *J. Phys. Chem. C*, 2008, **112**, 16869–16878.
234 P.-G. Ren, D.-X. Yan, X. Ji, T. Chen and Z.-M. Li, *Nanotechnology*, 2011, **22**, 055705.
235 D. Yang, A. Velamakanni, G. Bozoklu, S. Park, M. Stoller, R. D. Piner, S. Stankovich, I. Jung, D. A. Field, C. A. Ventrice and R. S. Ruoff, *Carbon*, 2009, **47**, 145–152.
236 A. J. Bard and L. R. Faulkner, *Electrochemical Methods. Fundamentals and Applications*, USA, 2nd edn, 2001.
237 A. P. Brown and F. C. Anson, *Anal. Chem.*, 1977, **49**, 1589–1595.
238 E. Laviron, *J. Electroanal. Chem. Interfacial Electrochem.*, 1979, **101**, 19–28.
239 E. Laviron and L. Roullier, *J. Electroanal. Chem. Interfacial Electrochem.*, 1980, **115**, 65–74.
240 C. E. D. Chidsey, *Science*, 1991, **251**, 919–922.
241 M. Ohtani, *Electrochem. Commun.*, 1999, **1**, 488–492.
242 J. C. Myland and K. B. Oldham, *Electrochem. Commun.*, 2005, **7**, 282–287.
243 W. A. Marmisollé, M. I. Florit and D. Posadas, *J. Electroanal. Chem.*, 2011, **655**, 17–22.
244 W. A. Marmisollé, M. I. Florit and D. Posadas, *J. Electroanal. Chem.*, 2011, **660**, 26–30.
245 W. A. Marmisollé, M. I. Florit and D. Posadas, *J. Electroanal. Chem.*, 2013, **707**, 43–51.
246 W. A. Marmisollé, M. Inés Florit and D. Posadas, *Phys. Chem. Chem. Phys.*, 2010, **12**, 7536–7544.
247 D. Posadas, M. Fonticelli, M. J. Rodriguez Presa and M. I. Florit, *J. Phys. Chem. B*, 2001, **105**, 2291–2296.
248 D. Posadas and M. I. Florit, *J. Phys. Chem. B*, 2004, **108**, 15470–15476.
249 S. K. Arya, A. Dey and S. Bhansali, *Biosens. Bioelectron.*, 2011, **28**, 166–173.
250 A. Kaushik, A. Vasudev, S. K. Arya and S. Bhansali, *Biosens. Bioelectron.*, 2013, **50**, 35–41.
251 N. Ruecha, R. Rangkupan, N. Rodthongkum and O. Chailapakul, *Biosens. Bioelectron.*, 2014, **52**, 13–19.
252 Q. Zhang, A. Prabhu, A. San, J. F. Al-Sharab and K. Levon, *Biosens. Bioelectron.*, 2015, **72**, 100–106.
253 A. M. Bonastre, M. Sosna and P. N. Bartlett, *Phys. Chem. Chem. Phys.*, 2011, **13**, 5365–5372.
254 P. N. Bartlett and E. N. K. Wallace, *Phys. Chem. Chem. Phys.*, 2001, **3**, 1491–1496.
255 L. Nyholm and L. M. Peter, *J. Chem. Soc., Faraday Trans.*, 1994, **90**, 149–154.
256 B. E. Conway, *Electrochemical supercapacitors: scientific fundamentals and technological applications*, Springer, 1999.
257 Y. G. Majid Beidaghi, *Energy Environ. Sci.*, 2014, **7**, 867–884.
258 C. Zhong, Y. Deng, W. Hu, J. Qiao, L. Zhang and J. Zhang, *Chem. Soc. Rev.*, 2015, **44**, 7484–7539.
259 E. Frackowiak, *Phys. Chem. Chem. Phys.*, 2007, **9**, 1774–1785.
260 L. L. Zhang, R. Zhou and X. S. Zhao, *J. Mater. Chem.*, 2010, **20**, 5983–5992.
261 G. A. Snook, P. Kao and A. S. Best, *J. Power Sources*, 2011, **196**, 1–12.
262 Q. Wu, Y. Xu, Z. Yao, A. Liu and G. Shi, *ACS Nano*, 2010, **4**, 1963–1970.
263 J. Xu, K. Wang, S. Z. Zu, B. H. Han and Z. Wei, *ACS Nano*, 2010, **4**, 5019–5026.
264 K. Zhang, L. L. Zhang, X. S. Zhao and J. Wu, *Chem. Mater.*, 2010, **22**, 1392–1401.

